irradiation. The AMF was applied for 30 min. The tumor temperature reached 43°C within 3 min and was maintained at 43°C by controlling the magnetic field intensity. By contrast, the rectal temperature remained at 36°C. These results indicate that a hyperthermia system using NPrCAP/M is able to selectively heat the tumor. In addition, the tumor temperature was maintained precisely within a small standard deviation, thus demonstrating the ease of temperature control by adjusting the magnetic field intensity. Figure 1B shows tumor weight on day 17. Tumor growth was significantly suppressed by NPrCAP/M-mediated

hyperthermia treatment. In this study, we set the tumor temperature at 43°C and hyperthermia was applied once a day every other day for a total of three treatments, although this was insufficient to achieve complete regression of the B16 melanoma. The NPrCAP/M-mediated hyperthermia system can generate higher temperatures. For example, complete regression of B16 melanoma was observed in 90% of mice at 46°C applied once daily for 2 days [34]. In the present study, we employed relatively moderate conditions for hyperthermia treatment because the heat-generated immunological effect was more significant at 43°C than at 46°C [23]. In agreement with previous results [22,23], substantial amounts of CD8⁺ T cells were observed around the tumor (Figure 1C) and slightly within the tumor (Figure 1D) on day 17, while few or no CD8⁺ T cells were observed around and within the tumor of untreated tumor-bearing mice (without NPrCAP/M injection; data not shown) and NPrCAP/M-injected mice without AMF exposure (data not shown).
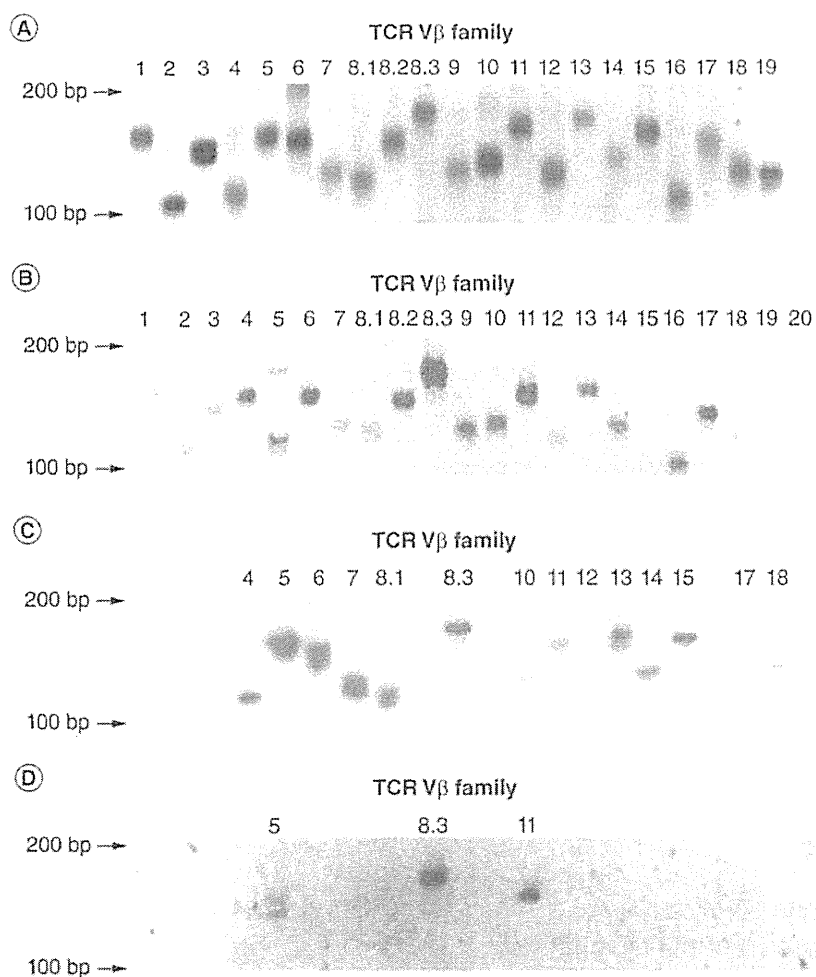

Lymph node enlargement after NPrCAP/M-mediated hyperthermia

As shown in Figure 2B, enlargement of inguinal DLNs was observed after NPrCAP/M-mediated hyperthermia compared with inguinal non-DLNs on day 17 (Figure 2A). As lymph node enlargement is consistently observed in situations of tumor involvement [35], significant enlargement of inguinal DLNs was observed in all tumor-bearing mice, including untreated mice and NPrCAP/M-injected mice (Figure 2C). In particular, the inguinal DLNs of tumor-bearing mice treated with NPrCAP/M-mediated hyperthermia were drastically enlarged compared with those of naive mice. The lymph node enlargement may have been due to an increased homing of circulating T cells in response to tumor antigen, and specific T-cell clones may have expanded and differentiated in the DLNs of tumor-bearing mice. We thus compared the number of CD8⁺ T cells in inguinal lymph nodes of naive mice and inguinal DLNs of tumor-bearing mice treated with NPrCAP/M-mediated hyperthermia. As shown in Figure 2D, the number of CD8⁺ T cells in inguinal DLNs increased significantly in the mice treated with NPrCAP/M-mediated hyperthermia on day 17.

TCR repertoires of TILs after NPrCAP/M-mediated hyperthermia

Figure 3 shows representative photographs of the TCR repertoire analysis of an inguinal

Figure 3. T-cell receptor β-chain gene expression in tumor-infiltrating lymphocytes after *N*-propionyl-4-*S*-cysteaminylphenol/magnetite-mediated hyperthermia. Analysis of each specimen included 22 separate electrophoreses of DNA amplified with different primer sets of each TCR Vβ family gene-specific oligonucleotide. Representative results from Vβ amplifications of T cells in single mice are shown. **(A)** Inguinal lymph node from a naive mouse. **(B)** Inguinal draining lymph node from untreated tumor-bearing mice. **(C)** Inguinal draining lymph node from the mice treated with hyperthermia. **(D)** Tumor from the mice treated with hyperthermia. The TCR Vβ family number is shown above each lane where bands were observed. TCR: T-cell receptor.

lymph node from single mice. In a naive mouse (Figure 3A), *TCR* gene expressions of all 21 displayable Vβ families, with the exception of Vβ20, were observed. In DLN from untreated tumor-bearing mice (Figure 3B), expressions of 19 *TCR Vβ* genes of 21 Vβ families were observed. In tumor samples from untreated tumor-bearing mice, however, no *TCR* gene expression was observed (data not shown), indicating that few TILs were present in the tumors without hyperthermia treatment. On the other hand, the TCR Vβ repertoire was restricted in the DLNs from the tumor-bearing mouse treated with NPrCAP/M-mediated hyperthermia, and expressions of 14 *TCR Vβ* genes of 21 Vβ families were observed (Figure 3C). The TCR repertoire was further restricted in the TILs from tumor samples treated with NPrCAP/M-mediated hyperthermia, and *TCR* gene expression in Vβ-5, -8.3 and -11 was observed in a single mouse (Figure 3D), suggesting the clonal expansion of TILs upon antigen recognition. It is believed that the V(D) J junctional sequences are unique to each T-cell clonotype and contribute to TCR diversity. Figure 4 shows the sequences of V(D)J junctions of the TCR β chains. For DNA sequencing, the tumor samples from five mice were mixed and analyzed, and we obtained one Vβ6, five Vβ8.2, six Vβ11 and one Vβ15 clone derived from PCR products. Sequence analysis of the PCR clones from TILs revealed a frame shift in the V(D)J region of the *TCR Vβ15* clone (data not shown), suggesting that *TCR Vβ15* would not be functionally generated in this clone. All five *TCR Vβ8.2* clones possessed an identical sequence (Figure 4B). On the other hand, sequence analysis revealed that *TCR Vβ11* clones comprised two distinct *Jβ* genes, *Jβ2-3* (three of six clones) and *Jβ2-7* (three of six clones), and three distinct N-Dβ-N regions (Figure 4C), indicating oligoclonal expansion of *TCR Vβ11* T cells in the tumor.

Restricted usage of *TCR V* genes by T cells that recognize tumor antigens is controversial. In some studies, limited *TCR V* gene usage was found [36,37], while other reports demonstrated diverse *TCR V* usage by TILs [38,39]. In the present study, the TCR Vβ repertoire was limited in TILs from mice that underwent hyperthermia (Figure 3), suggesting that TILs were specifically reactive against tumor antigens. However, the use of the TCR Vβ family was not restricted in several experiments, including the results shown in Figure 3 (Vβ-5, -8.3 and -11) and Figure 4 (Vβ-6, -8.2, -11 and -15). On the

other hand, Vβ11 gene expression was primarily found in several experiments (data not shown). In addition to the qualitative analysis of Vβ11 gene expression by reverse-transcription PCR (Figures 3 & 4), flow cytometric analysis revealed a quantitative increase in CD8⁺/TCR Vβ11⁻ TILs (Figure 5A–5C). Harada *et al.* established a B16 melanoma-specific CD8⁺ T-cell line, AB1, from the spleen cells of mice cured of B16 melanoma with IL-12 treatment [40]. The AB1 cells exclusively expressed *TCR Vβ11*. These results suggest that clonal expansion of Vβ11⁺ TILs can be a useful marker to investigate the T-cell response to B16 melanoma. The AB1 cells could also recognize TRP-2 peptide as well as B16 melanoma cells. Moreover, Singh *et al.* generated a TRP-2 peptide-specific CD8⁺ T-cell clone, and spectratype analysis revealed that the cell clone expressed Vβ11 [41]. We thus investigated the reactivity of TILs to melanoma-associated antigens. Lymphocytes from DLNs in tumor-bearing mice treated with hyperthermia using NPrCAP/M were stimulated with the immunodominant peptides of the mouse melanoma-associated antigens TRP-1, TRP-2 or glycoprotein 100, as well as B16F1 cells treated with mitomycin C. These peptide-stimulated lymphocytes were tested

(A) Vβ6	N-Dβ-N	Jβ1-1	Frequency
TGTGCCAGCAG C A S S	CCCTGGACGG P G R	AACACAGAA N T E	1/1

(B) Vβ8.2	N-Dβ-N	Jβ2-4	Frequency
GCCAGCGGTG A S G	CAGACAGT A D S	AGTCAAAAC S Q N	5/5

(C) Vβ11	N-Dβ-N	Jβ2-7	Frequency
GCAAGCAGCTTAGA A S S L E	ACTGGGGGGGCGA L G G R	GAACAGTAC E Q Y	3/6
		Jβ2-3	
GCAAGCAGC A S S	TCACTGCTT S L L	AGTGCAGAA S A E	1/6
		Jβ2-3	
GCAAGCAGC A S S	TCACTGTTT S L F	AGTGCAGAA S A E	2/6

Figure 4. T-cell receptor β junctional sequences from tumor-infiltrating lymphocytes in the mice treated with N-propionyl-4-S-cysteaminylphenol/magnetite-mediated hyperthermia. (A–C) Nucleotide and predicted amino acid sequences from V(D)J regions of **(A)** *TCR Vβ6*, **(B)** *Vβ8.2* and **(C)** *Vβ11*. Tumor samples from five mice were mixed and analyzed. The amplified PCR products of the *TCR Vβ* gene were cloned into the plasmid vector. Six or as many as possible randomly picked colonies were analyzed, and the plasmid DNA from the positive colonies was sequenced.
D: Diversity; J: Joining; V: Variable.

for the ability to recognize the antigens by releasing IFN-γ as an assay to detect T cells with high avidity toward the tumor antigen. As shown in FIGURE 5D, only the lymphocytes stimulated with TRP-2 peptide displayed a significant IFN-γ release, suggesting restricted reactivity toward the TRP-2 antigen. A further important point is whether TRP-2 peptide can be used to boost anti-tumor immunity induced by NPrCAP/M-mediated hyperthermia. One direction for future research might be the development of a combination therapy of NPrCAP/M-mediated hyperthermia with a TRP-2 peptide vaccine.

To the best of our knowledge, this is the first report to determine the V(D)J junctional sequence of the *TCR Vβ11* gene of TILs in B16 melanoma. This information is very useful, not only to understand the T-cell response to B16 melanoma, but also to develop more effective cancer immunotherapy. Immunotherapy with adoptive cell transfer using TILs has proven to be a useful strategy for the treatment of metastatic melanoma [42]. Recent strategies involve cloning of *TCR αβ* genes specific for melanoma-associated antigens from TILs and retrovirally transducing these genes into peripheral blood lymphocytes [43]. Information on Vβ11 usage
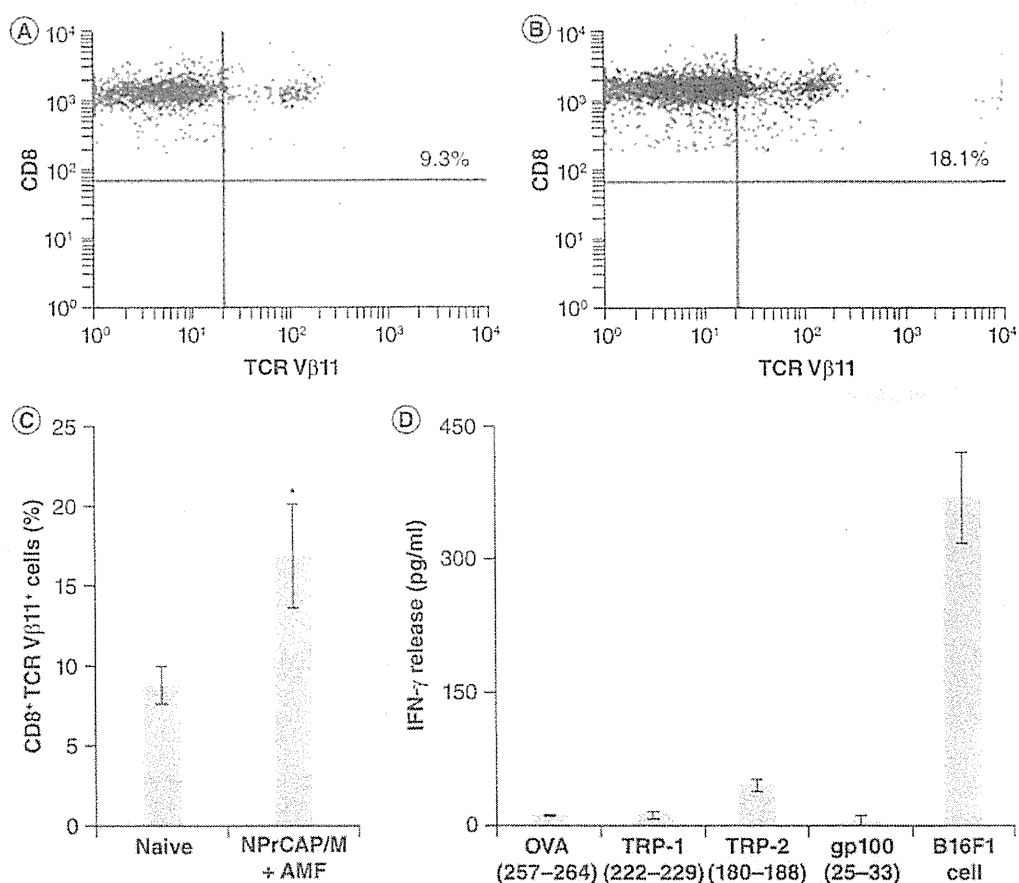

Figure 5. T-cell response in the mice treated with *N*-propionyl-4-*S*-cysteaminylphenol/ magnetite-mediated hyperthermia. (A–C) Flow cytometric analysis of CD8⁺/TCR Vβ11⁺ T cells in (A) an inguinal lymph node of a naive mouse and (B) an inguinal draining lymph node of a mouse treated with NPrCAP/M-mediated hyperthermia. CD8⁺ T cells in the lymph node were purified by magnetic cell sorting, and the representative data from (A & B) single mice and (C) five mice for statistical analysis are shown. Data are the means and standard deviations. (D) T-cell response to melanoma-associated antigen peptides. After the hyperthermia treatment, draining lymph nodes from five mice were harvested on day 17, and lymphocytes were then restimulated *in vitro* with antigen peptides or mitomycin-treated B16F1 cells for 5 days. OVA$_{257-264}$ peptide was used as a negative control. After the restimulation, culture supernatants were collected and amounts of IFN-γ were measured by ELISA. Data are the means and standard deviations of triplicate experiments. *p < 0.01.
AMF: Alternating magnetic field; gp: Glycoprotein; NPrCAP/M: *N*-propionyl-4-*S*-cysteaminylphenol/magnetite; OVA: Ovalbumin; TCR: T-cell receptor; TRP: Tyrosinase-related protein.

in TILs and the V(D)J junctional sequence will be useful to further determine the Vα gene for reconstitution of functional T cells by *TCR αβ* gene transfer. We are now determining the *Vα* gene to reconstitute functional T cells to investigate whether Vβ11⁺ TILs are CTLs that actually play a crucial role in *in vivo* immune responses against B16 melanoma, and whether adoptive immunotherapy using *TCR* gene-engineered CTLs is possible to enhance the therapeutic effects of NPrCAP/M-mediated hyperthermia.

Conclusion

In this study, we analyzed the diversity of TCRs in TILs after NPrCAP/M-mediated hyperthermia. It was found that T cells were clonally expanded in B16 tumors after hyperthermia, in which Vβ11⁺ T cells were preferentially expanded. The DNA sequences of the CDR3 of the TCR β-chain in TILs revealed the presence of clonally expanded T cells. These results indicate that the T-cell response in B16 melanoma after hyperthermia is dominated by T cells directed toward a limited number of epitopes and that epitope-specific T cells frequently use a restricted TCR repertoire.

Future perspective

Although early lesions of primary melanoma are curable by excision, successful treatment of metastatic melanoma has been elusive. Recently, the authors have proceeded to a Phase I/II study of the effect of NPrCAP/M-mediated hyperthermia not only on treated primary tumors but also on nontreated metastatic tumors [44]. The therapeutic protocol followed the animal experiments. However, NPrCAP/M was made by conjugating polyethylene glycol between NPrCAP and magnetite nanoparticles, and a new AMF applicator called a 'ferrite core-inserted solenoid type' [11] was utilized in the clinical trials. The future potential use of this technology is illustrated in Figure 6.
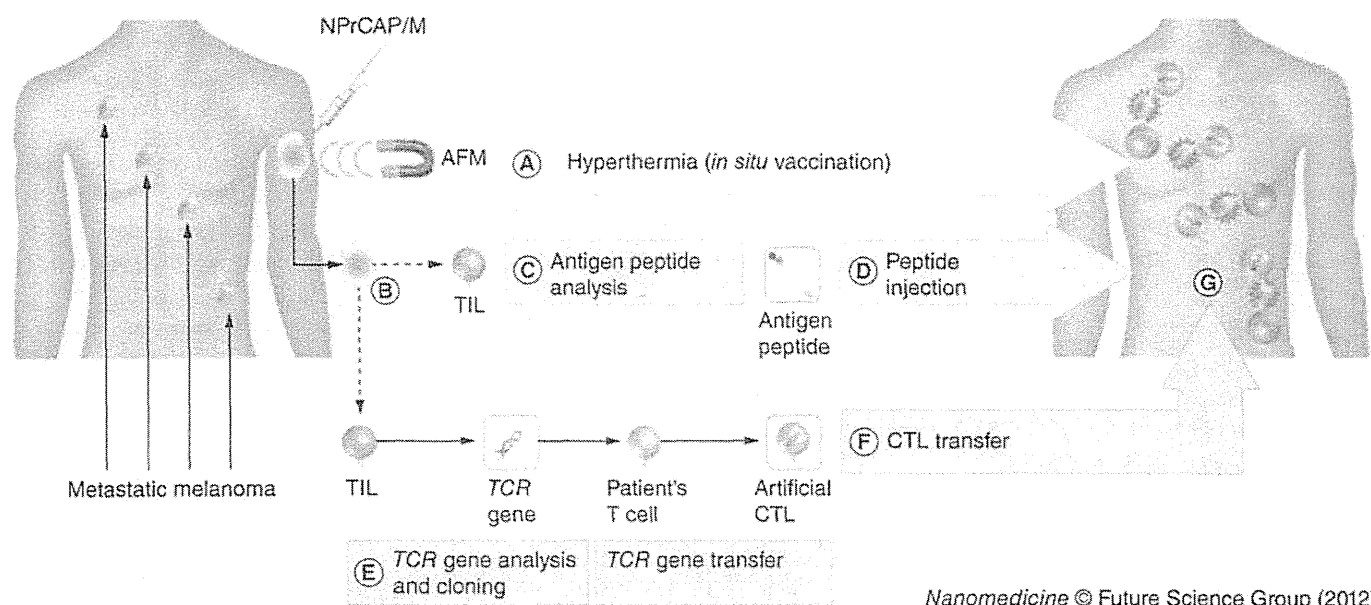

Figure 6. Future potential of *N*-propionyl-4-*S*-cysteaminylphenol/magnetite-mediated hyperthermia for melanoma-targeted thermo-immunotherapy. This strategy is based on combinations of hyperthermia using NPrCAP/M with antimelanoma peptide vaccine and *TCR* gene-engineered CTL therapy. (A) NPrCAP/M-mediated hyperthermia system confers anti-tumor immunity via release of heat-shock protein–peptide complexes during necrotic tumor cell death *in vivo*, which we have termed '*in situ* vaccination'. (B) The primary melanoma is exploited to provide tumor antigens to the immune system for 2 weeks, and then the melanoma is excised surgically to analyze TILs. (C) Melanoma-specific antigen peptides are analyzed by using TILs. (D) The screened peptides can be used to boost anti-tumor immunity induced by hyperthermia. For mouse B16 melanoma, TRP-2 peptide will be used to boost anti-tumor immunity induced by NPrCAP/M-mediated hyperthermia. (E) *TCR* genes of TILs are analyzed and cloned. (F) Adoptive immunotherapy using *TCR* gene-engineered CTL therapy will enhance the therapeutic effects of NPrCAP/M-mediated hyperthermia. For B16 melanoma, DNA sequences of TCRb CDR3 of TILs (see Figure 4) can be used. (G) Taken together, the combination of antimelanoma peptide vaccine and TCR gene-engineered CTL therapy with NPrCAP/M-mediated hyperthermia is a promising treatment for improving clinical effects, especially for patients with early metastatic melanomas because of the induction of systemic antimelanoma immunity. AMF: Alternating magnetic field; CTL: Cytotoxic T lymphocyte; NPrCAP/M: *N*-propionyl-4-*S*-cysteaminylphenol/magnetite; TCR: T-cell receptor; TIL: Tumor-infiltrating lymphocyte.

Executive summary

Hyperthermia using N-propionyl-4-S-cysteaminylphenol/magnetite for melanoma

- Hyperthermia using *N*-propionyl-4-*S*-cysteaminylphenol/magnetite (NPrCAP/M) was able to selectively heat transplanted melanomas by direct injection of NPrCAP/M.
- Tumor growth was significantly suppressed by the treatment of NPrCAP/M-mediated hyperthermia.

Anti-tumor immunity induced by NPrCAP/M-mediated hyperthermia

- CD8$^+$ T cells were infiltrated within the tumor after hyperthermia.
- Lymph node enlargement was observed after hyperthermia.

T-cell receptor repertoire analysis of tumor-infiltrating lymphocytes after NPrCAP/M-mediated hyperthermia

- Restricted T-cell receptor repertoire was observed in the tumor-infiltrating lymphocytes (TILs).
- Expansion of Vβ11$^+$ T cells was primarily found in the TILs.
- DNA sequences of T-cell receptor β CDR3 of TILs were identified.

References

Papers of special note have been highlighted as:
- of interest
- of considerable interest

1   Dewhirst MW, Prosnitz L, Thrall D *et al.* Hyperthermic treatment of malignant diseases: current status and a view toward the future. *Semin. Oncol.* 24(6), 616–625 (1997).

2   van der Zee J. Heating the patient: a promising approach? *Ann. Oncol.* 13(8), 1173–1184 (2002).

3   Sheeterle LM, St Cyr JA. Whole body hyperthermia as a potential therapeutic option. *Cancer Biother.* 10(4), 253–256 (1995).

4   Storm FK, Morton DL, Kaiser LR *et al.* Clinical radiofrequency hyperthermia: a review. *Natl Cancer Inst. Monogr.* 61, 343–350 (1982).

5   Gazeau F, Lévy M, Wilhelm C. Optimizing magnetic nanoparticle design for nanothermotherapy. *Nanomedicine (Lond.)* 3(6), 831–844 (2008).

•• Comprehensive review of hyperthermia using magnetite nanoparticles, including anti-tumor immune response induced by hyperthermia.

6   Jordan A, Scholz R, Wust P *et al.* Effects of magnetic fluid hyperthermia (MFH) on C3H mammary carcinoma *in vivo. Int. J. Hyperthermia* 13(6), 587–605 (1997).

7   Ito A, Shinkai M, Honda H *et al.* Medical application of functionalized magnetic nanoparticles. *J. Biosci. Bioeng.* 100(1), 1–11 (2005).

8   Jordan A, Wust P, Fähling H *et al.* Inductive heating of ferrimagnetic particles and magnetic fluids: physical evaluation of their potential for hyperthermia. *Int. J. Hyperthermia.* 9(1), 51–68 (1993).

-   First paper describing physical mechanisms of hyperthermia using magnetite nanoparticles.

9   Ito A, Kuga Y, Honda H *et al.* Magnetite nanoparticle-loaded anti-HER2 immunoliposomes for combination of antibody therapy with hyperthermia. *Cancer Lett.* 212(2), 167–175 (2004).

10 Cole AJ, Yang VC, David AE. Cancer theranostics: the rise of targeted magnetic nanoparticles. *Trends Biotechnol.* 29(7), 323–332 (2011).

11 Kawai N, Ito A, Nakahara Y *et al.* Complete regression of experimental prostate cancer in nude mice by repeated hyperthermia using magnetite cationic liposomes and a newly developed solenoid containing a ferrite core. *Prostate* 66(7), 718–727 (2006).

12 Gneveckow U, Jordan A, Scholz R *et al.* Description and characterization of the novel hyperthermia- and thermoablation-system MFH 300F for clinical magnetic fluid hyperthermia. *Med. Phys.* 31(6), 1444–1451 (2004).

13 Thiesen B, Jordan A. Clinical applications of magnetic nanoparticles for hyperthermia. *Int. J. Hyperthermia.* 24(6), 467–474 (2008).

14 Shinkai M, Le B, Honda H *et al.* Targeting hyperthermia for renal cell carcinoma using human MN antigen-specific

magnetoliposomes. *Jpn. J. Cancer Res.* 92(10), 1138–1145 (2001).

15 Gupta AK, Naregalkar RR, Vaidya VD *et al.* Recent advances on surface engineering of magnetic iron oxide nanoparticles and their biomedical applications *Nanomedicine (Lond.)* 2(1), 23–39 (2007).

-   Review of procedures for synthesis and surface coating of magnetite nanoparticles.

16 Yiu HH. Engineering the multifunctional surface on magnetic nanoparticles for targeted biomedical applications: a chemical approach. *Nanomedicine (Lond.)* 6(8), 1429–1446 (2011).

17 Thomas PD, Kishi H, Cao H *et al.* Selective incorporation and specific cytocidal effect as the cellular basis for the antimelanoma action of sulphur containing tyrosine analogs. *J. Invest. Dermatol.* 113(6), 928–934 (1999).

18 Sato M, Yamashita T, Ohkura M *et al.* *N*-propionyl-cysteaminylphenol-magnetite conjugate (NPrCAP/M) is a nanoparticle for the targeted growth suppression of melanoma cells. *J. Invest. Dermatol.* 129(9), 2233–2241 (2009).

19 Johannsen M, Gneveckow U, Eckelt L *et al.* Clinical hyperthermia of prostate cancer using magnetic nanoparticles: presentation of a new interstitial technique. *Int. J. Hyperthermia* 21(7), 637–647 (2005).

20 Ito A, Shinkai M, Honda H *et al.* Heat shock protein 70 expression induces antitumor immunity during intracellular hyperthermia using magnetite nanoparticles. *Cancer Immunol. Immunother.* 52(2), 80–88 (2003).

21 Ito A, Honda H, Kobayashi T. Cancer immunotherapy based on intracellular hyperthermia using magnetite nanoparticles: a novel concept of 'heat-controlled necrosis' with heat shock protein expression. *Cancer Immunol. Immunother.* 55(3), 320–328 (2006).

22 Sato A, Tamura Y, Sato N *et al.* Melanoma-targeted chemo-thermo-immuno (CTI)-therapy using *N*-propionyl-4-*S*-cysteaminylphenol-magnetite nanoparticles elicits CTL response via heat shock protein–peptide complex release. *Cancer Sci.* 101(9), 1939–1946 (2010).

23 Takada T, Yamashita T, Sato M *et al.* Growth inhibition of re-challenge B16 melanoma transplant by conjugates of melanogenesis substrate and magnetite nanoparticles as the basis for developing melanoma-targeted chemo-thermo-immunotherapy. *J. Biomed. Biotechnol.* 457936 (2009).

24 Galon J, Costes A, Sanchez-Cabo F *et al.* Type, density, and location of immune cells within human colorectal tumors predict clinical outcome. *Science* 313(5795), 1960–1964 (2006).

25 Davis MM, Bjorkman PJ. T-cell antigen receptor genes and T-cell recognition. *Nature* 334(6181), 395–402 (1988).

26 Harrell MI, Iritani BM, Ruddell A. Lymph node mapping in the mouse. *J. Immunol. Methods* 332(1–2), 170–174 (2008).

27 Hindley JP, Ferreira C, Jones E *et al.* Analysis of the T-cell receptor repertoires of tumor-infiltrating conventional and regulatory T cells reveals no evidence for conversion in carcinogen-induced tumors. *Cancer Res.* 71(3), 736–746 (2011).

28 Godebu E, Summers-Torres D, Lin MM *et al.* Polyclonal adaptive regulatory CD4 cells that can reverse Type 1 diabetes become oligoclonal long-term protective memory cells. *J. Immunol.* 181(3), 1798–1805 (2008).

29 Böhm W, Thoma S, Leithäuser F *et al.* T cell-mediated, IFN-gamma-facilitated rejection of murine B16 melanomas. *J. Immunol.* 161(2), 897–908 (1998).

30 Dyall R, Bowne WB, Weber LW *et al.* Heteroclitic immunization induces tumor immunity. *J. Exp. Med.* 188(9), 1553–1561 (1998).

31 Bloom MB, Perry-Lalley D, Robbins PF *et al.* Identification of tyrosinase-related protein 2 as a tumor rejection antigen for the B16 melanoma. *J. Exp. Med.* 185(3), 453–459 (1997).

32 Zhai Y, Yang JC, Spiess P *et al.* Cloning and characterization of the genes encoding the murine homologues of the human melanoma antigens MART1 and gp100. *J. Immunother.* 20(1), 15–25 (1997).

33 Rötzschke O, Falk K, Stevanović S *et al.* Exact prediction of a natural T cell epitope. *Eur. J. Immunol.* 21(11), 2891–2894 (1991).

34 Suzuki M, Shinkai M, Honda H *et al.* Anticancer effect and immune induction by hyperthermia of malignant melanoma using magnetite cationic liposomes. *Melanoma Res.* 13(2), 129–135 (2003).

35 Salameire D, Le Bris Y, Fabre B *et al.* Efficient characterization of the TCR repertoire in lymph nodes by flow cytometry. *Cytometry A* 75(9), 743–751 (2009).

• Large-scale analysis of the T-cell receptor (TCR) repertoire in lymph nodes using flow cytometry.

36 Nitta T, Oksenberg JR, Rao NA *et al.* Predominant expression of T cell receptor V alpha 7 in tumor-infiltrating lymphocytes of uveal melanoma. *Science* 249(4969), 672–674 (1990).

•• Analysis of *TCR Vα* gene expression in tumor-infiltrating lymphocytes within human melanoma.

37 Solheim JC, Alexander-Miller MA, Martinko JM *et al.* Biased T cell receptor usage by Ld-restricted, tum-peptide-specific cytotoxic T lymphocyte clones. *J. Immunol.* 150(3), 800–811 (1993).

38 Ferradini L, Roman-Roman S, Azocar J *et al.* Analysis of T-cell receptor alpha/beta variability in lymphocytes infiltrating a melanoma metastasis. *Cancer Res.* 52(17), 4649–4654 (1992).

39 Shilyansky J, Nishimura MI, Yannelli JR *et al.* T-cell receptor usage by melanoma-specific clonal and highly oligoclonal tumor-infiltrating lymphocyte lines. *Proc. Natl Acad. Sci. USA* 91(7), 2829–2833 (1994).

• Analysis of the diversity of TCRs involved in human melanoma antigen recognition.

40 Harada M, Tamada K, Abe K *et al.* Characterization of B16 melanoma-specific cytotoxic T lymphocytes. *Cancer Immunol. Immunother.* 47(4), 198–204 (1998).

• Establishment of B16 melanoma-specific CTL clone characterized by TCR Vβ11 expression and TRP-2 peptide antigen-specific cytotoxicity.

41 Singh V, Ji Q, Feigenbaum L *et al.* Melanoma progression despite infiltration by *in vivo*-primed TRP-2-specific T cells. *J. Immunother.* 32(2), 129–139 (2009).

42 Rosenberg SA, Restifo NP, Yang JC *et al.* Adoptive cell transfer: a clinical path to effective cancer immunotherapy. *Nat. Rev. Cancer* 8(4), 299–308 (2008).

43 Park TS, Rosenberg SA, Morgan RA. Treating cancer with genetically engineered T cells. *Trends Biotechnol.* 29(11), 550–557 (2011).

•• Review of *TCR* gene-engineered T cells.

44 Jimbow K, Tamura Y, Yoneta A *et al.* Conjugation of magnetite nanoparticles with melanogenesis substrate, NPrCAP provides melanoma targeted, *in situ* peptide vaccine immunotherapy through HSP production by chemo-thermotherapy. *J. Biomater. Nanobiotechnol.* 3(2), 140–153 (2012).

Affiliations

• Akira Ito
Department of Chemical Engineering, Faculty of Engineering, Kyushu University, 744 Motooka, Nishi-ku, Fukuoka 819-0395, Japan

• Masaki Yamaguchi
Department of Chemical Engineering, Faculty of Engineering, Kyushu University, 744 Motooka, Nishi-ku, Fukuoka 819-0395, Japan

• Noriaki Okamoto
Department of Chemical Engineering, Faculty of Engineering, Kyushu University, 744 Motooka, Nishi-ku, Fukuoka 819-0395, Japan

• Yuji Sanematsu
Department of Chemical Engineering, Faculty of Engineering, Kyushu University, 744 Motooka, Nishi-ku, Fukuoka 819-0395, Japan

• Yoshinori Kawabe
Department of Chemical Engineering, Faculty of Engineering, Kyushu University, 744 Motooka, Nishi-ku, Fukuoka 819-0395, Japan

• Kazumasa Wakamatsu
Department of Chemistry, Fujita Health University School of Health Sciences, Toyoake 470-1192, Japan

• Shosuke Ito
Department of Chemistry, Fujita Health University School of Health Sciences, Toyoake 470-1192, Japan

• Hiroyuki Honda
Department of Biotechnology, School of Engineering, Nagoya University, Nagoya 464-8603, Japan

• Takeshi Kobayashi
School of Bioscience and Biotechnology, Chubu University, Kasugai 487-8501, Japan

• Eiichi Nakayama
Faculty of Health and Welfare, Kawasaki University of Medical Welfare, Kurasiki 701-0193, Japan

- Yasuaki Tamura
First Department of Pathology, Sapporo
Medical University School of Medicine,
Sapporo 060-8556, Japan

- Masae Okura
Department of Dermatology, Sapporo
Medical University School of Medicine,
Sapporo 060-8543, Japan

- Toshiharu Yamashita
Department of Dermatology, Sapporo
Medical University School of Medicine,
Sapporo 060-8543, Japan

- Kowichi Jimbow
Department of Dermatology, Sapporo
Medical University School of Medicine,
Sapporo 060-8543, Japan

- Masamichi Kamihira
Department of Chemical Engineering,
Faculty of Engineering, Kyushu University,
744 Motooka, Nishi-ku, Fukuoka 819-0395,
Japan

Vaccine 31 (2013) 2110–2118

Contents lists available at SciVerse ScienceDirect

Vaccine

journal homepage: www.elsevier.com/locate/vaccine

Establishment of animal models to analyze the kinetics and distribution of human tumor antigen-specific CD8+ T cells

Daisuke Muraoka [a,d], Hiroyoshi Nishikawa [a,e,*], Takuro Noguchi [a,f], Linan Wang [b], Naozumi Harada [a,d], Eiichi Sato [g], Immanuel Luescher [h], Eiichi Nakayama [i], Takuma Kato [c], Hiroshi Shiku [a,b,1]

[a] Departments of Cancer Vaccine, Mie University Graduate School of Medicine, Mie 514-8507, Japan
[b] Departments of Immuno-Gene Therapy, Mie University Graduate School of Medicine, Mie 514-8507, Japan
[c] Departments of Cellular and Molecular Immunology, Mie University Graduate School of Medicine, Mie 514-8507, Japan
[d] Immunofrontier, Inc., Tokyo, 143-0023, Japan
[e] Experimental Immunology, Immunology Frontier Research Center, Osaka University, Osaka, 565-0871, Japan
[f] Ludwig Institute for Cancer Research, New York Branch, Memorial Sloan-Kettering Cancer Center, New York, NY 10065, United States
[g] Department of Anatomic Pathology, Tokyo Medical University, Tokyo, 160-8402, Japan
[h] Ludwig Institute for Cancer Research, Lausanne Branch, University of Lausanne, Epalinges, 1066, Switzerland
[i] Faculty of Health and Welfare, Kawasaki University of Medical Welfare, Okayama, 701-0193, Japan

ARTICLE INFO

ABSTRACT

Many patients develop tumor antigen-specific T cell responses detectable in peripheral blood mononuclear cells (PBMCs) following cancer vaccine. However, measurable tumor regression is observed in a limited number of patients receiving cancer vaccines. There is a need to re-evaluate systemically the immune responses induced by cancer vaccines. Here, we established animal models targeting two human cancer/testis antigens, NY-ESO-1 and MAGE-A4. Cytotoxic T lymphocyte (CTL) epitopes of these antigens were investigated by immunizing BALB/c mice with plasmids encoding the entire sequences of NY-ESO-1 or MAGE-A4. CD8+ T cells specific for NY-ESO-1 or MAGE-A4 were able to be detected by ELISPOT assays using antigen presenting cells pulsed with overlapping peptides covering the whole protein, indicating the high immunogenicity of these antigens in mice. Truncation of these peptides revealed that NY-ESO-1-specific CD8+ T cells recognized D^d-restricted 8mer peptides, NY-ESO-1$_{81-88}$. MAGE-A4-specific CD8+ T cells recognized D^d-restricted 9mer peptides, MAGE-A4$_{265-273}$. MHC/peptide tetramers allowed us to analyze the kinetics and distribution of the antigen-specific immune responses, and we found that stronger antigen-specific CD8+ T cell responses were required for more effective anti-tumor activity. Taken together, these animal models are valuable for evaluation of immune responses and optimization of the efficacy of cancer vaccines.

1. Introduction

A number of cancer vaccine strategies targeting tumor antigens recognized by the human immune system have been tested [1–3]. While many of these cancer vaccines elicited measurable

immune responses detectable in peripheral blood mononuclear cells (PBMCs), only a subset of treated patients experienced clinical benefits, such as tumor regression [4,5]. Because of the weak clinical effectiveness of currently available cancer vaccines, not only new immunogenic antigens, effective adjuvant formulations, vectors or vaccination methods but also new methodologies to evaluate efficacy of cancer vaccines are required.

NY-ESO-1, a germ line cell protein detected by SEREX (serological identification of antigens by recombinant expression cloning) using the serum of an esophageal cancer patient, is often expressed by cancer cells, but not by normal somatic cells [3,6]. This ideal expression pattern facilitated the study of this antigen; including immuno-monitoring of cancer patients with NY-ESO-1-expressing tumors and clinical trials that focused on NY-ESO-1 [3]. While these studies have revealed that a number of different cancer vaccines, including short and overlapping peptides, protein, viral vectors and DNA, resulted in development of measurable immune responses,

correlations between immunological and clinical responses were often week or difficult to observe [3].

MAGE-A4, another cancer/testis (CT) antigen, elicits MAGE-A4-specific CD4$^+$ and CD8$^+$ T cell responses in some patients with MAGE-A4-expressing cancers, indicating that MAGE-A4 is also an immunogenic protein [7–9]. We have recently reported a novel MAGE-A4 epitope presented by human leukocyte antigen (HLA)-A*2402 using a CD8$^+$ T cell clone 2-28 [9]. As this clone effectively killed tumor cell lines that expressed both MAGE-A4 and HLA-A*2402, this antigen could be a candidate for a cancer vaccine.

Given the poor correlation between the immune responses detected in PBMCs and clinical responses [2,3,5], it is necessary to re-evaluate existing cancer immunotherapy strategies in detail using animal models, namely reverse translational research. To this end, we developed animal models involving human tumor antigens, such as NY-ESO-1 or MAGE-A4 in this study.

2. Materials and methods

2.1. Mice

Female BALB/c mice were purchased from SLC Japan (Shizuoka, Japan) and used at 7–10 weeks of age. They were maintained at the Animal Center of Mie University Graduate School of Medicine (Mie, Japan). The experimental protocol was approved by the Ethics Review Committee for Animal Experimentation of Mie University Graduate School of Medicine.

2.2. Antibodies and reagents

Anti-H2-K^d (KD40, mouse IgG2a), anti-H2-D^d (DD98, mouse IgG2a), and anti-H2-L^d (30-5-7, mouse IgG2a) were produced and purified from each hybridoma. FITC-conjugated anti-CD8 mAb (53-6.7, rat IgG2a) and APC-conjugated anti-CD4 mAb (GK1.5, rat IgG2b) were purchased from BD Biosciences (Franklin Lakes, NJ). PE-conjugated anti-Foxp3 mAb (Fjk16s, rat IgG2a) was purchased from eBiosciences (San Diego, CA). Synthetic NY-ESO-1 and MAGE-A4 peptides (summarized in Supplementary Table 1) were obtained from Sigma Genosys (Hokkaido, Japan).

2.3. Immunization using a gene gun

Naive BALB/c mice were immunized twice at two-week intervals. Gold particles coated with 1 μg of each plasmid DNA were prepared and delivered into the shaved skin of the abdominal wall of BALB/c mice using a Helios Gene Gun System (BioRad, Hercules, CA) at a helium discharge pressure of 350–400 psi, as described previously [10,11].

2.4. Cell isolation

Spleen cell suspensions were mixed with CD8 Microbeads (Miltenyi Biotec, Bergisch Gladbach, Germany) and separated into CD8$^+$ T cells by positive selection on a MACS column. The isolated CD8$^+$ T cell populations were confirmed to contain >95% CD8$^+$ T cells.

2.5. Enzyme-linked immunospot (ELISPOT) assay

The number of IFN-γ secreting antigen-specific CD8$^+$ T cells was assessed by ELISPOT assay as described previously [10,11]. Briefly, purified CD8$^+$ T cells were cultured for 24 hours with 5×10^5 irradiated CD90-depleted splenocytes pulsed with the indicated peptides in 96-well nitrocellulose-coated microtiter plates (Millipore, Bedford, MA) coated with rat anti-mouse IFN-γ mAb (R4-6A2,

BD Biosciences). Spots were developed using biotinylated anti-mouse IFN-γmAb (XMG1.2, BD Biosciences), alkaline phosphatase conjugated streptavidin (MABTECH, Sweden) and alkaline phosphatase substrate kit (BioRad), and subsequently counted.

2.6. ELISA

96-well flat-bottomed microliter plates (Immuno-NUNC) were coated with 20 ng/50 μml of NY-ESO-1 or MAGE-A4 protein, respectively, at 4 °C overnight. Wells were blocked with 1% BSA/PBS for 1 hour at room temperature and washed three times. Serum (1:100 dilution) was added and incubated at 4 °C overnight. After washing, goat anti-mouse IgG antibody conjugated with horseradish peroxidase (Promega, Madison, WI) was added (1:5000 dilution). Two hours later, color was developed with TMB substrate solution (Thermo scientific, IL) and stopped with H$_2$SO$_4$. The absorbance was measured at 450 nm and calculated after subtraction of the absorbance value of control wells without sera.

2.7. Flow cytometry and tetramer staining

Tetramer staining was performed as described previously [11]. Briefly, cells were stained with PE-labeled NY-ESO-1$_{81-88}$/D^d or MAGE-A4$_{265-273}$/D^d tetramers (prepared at the Ludwig Institute Core Facility, Lausanne, Switzerland) for 10 minutes at 37 °C before additional staining of surface markers for 15 minutes at 4 °C. After washing, the results were analyzed on FACSCanto (BD Biosciences) and FlowJo software (Tree Star, Ashland, OR).

2.8. Tumors

CT26 is a colon epithelial tumor derived by intrarectal injections of N-nitroso-N-methylurethane in BALB/c mice [12]. CT26 expressing NY-ESO-1 or MAGE-A4, a human cancer/testis antigen were established as described previously [11,13].

2.9. Statistical analysis

Values were expressed as mean ± SD. Differences between groups were examined for statistical significance using the Student's t-test. p values <0.05 were considered statistically significant.

3. Results

3.1. NY-ESO-1-specific CD8$^+$ T cells recognize D^d-restricted NY-ESO-1$_{81-88}$ peptide

We analyzed the minimal epitope recognized by NY-ESO-1-specific CD8$^+$ T cells after immunization with NY-ESO-1. To this end, we employed a Helios Gene Gun System as we have previously detected NY-ESO-1-specific CD8$^+$ T cell responses [10,11]. To identify minimal epitopes, naive BALB/c mice were immunized twice at two-week intervals with plasmids encoding the entire sequence of NY-ESO-1. CD8$^+$ T cells were obtained from spleens and specific T cell responses were analyzed by ELISPOT assay using peptide pools shown in Supplementary Table 1. A significant number of NY-ESO-1-specific CD8$^+$ T cells was detected against peptide pool #3 (Fig. 1A). To identify the NY-ESO-1 epitope, NY-ESO-1-specific CD8$^+$ T cells were stimulated with each of these peptides. IFN-γ secretion was observed when NY-ESO-1-specific CD8$^+$ T cells were stimulated with 71–90 and 81–100 NY-ESO-1 peptides, suggesting the presence of a minimal epitope within 81–90 residues (Fig. 1B). To determine the minimal epitope, the 81–90 peptide of NY-ESO-1 was further truncated. NY-ESO-1-specific CD8$^+$ T cells recognized the 80–88 and 81–88, but not 80–87 or 82–88 peptides, thus
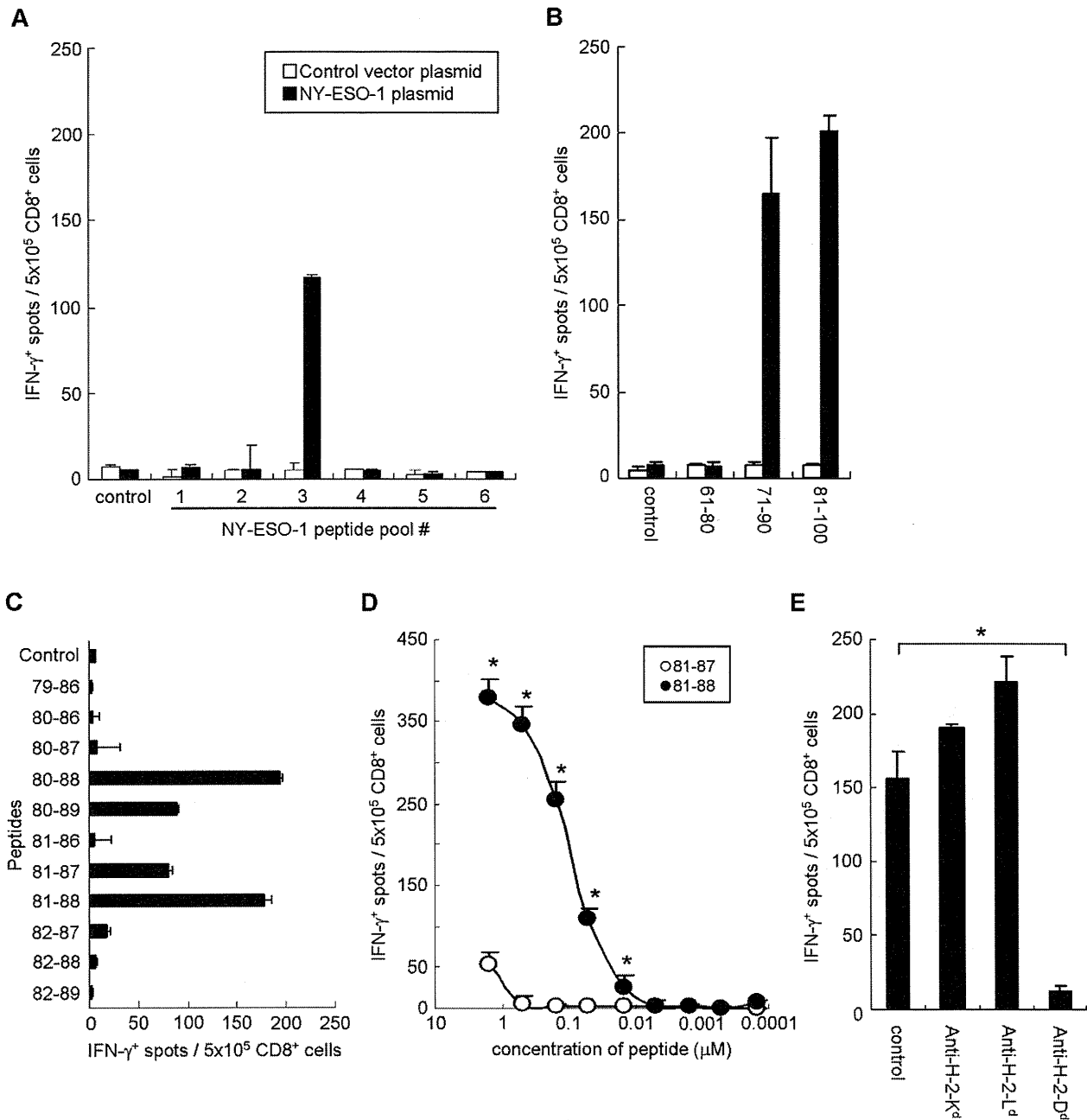
Fig. 1. NY-ESO-1-specific CD8+ T cells recognize D^d-restricted NY-ESO-1$_{81-88}$ peptide. (A–C) BALB/c mice were immunized by gene gun twice at two-week intervals with plasmids encoding the entire sequence of NY-ESO-1. CD8+ T cells were obtained from spleens and specific T cells were analyzed with ELISPOT assay using APCs pulsed with the indicated peptides. (D) Avidity of induced NY-ESO-1-specific CD8+ T cells was analyzed with ELISPOT assay using APCs pulsed with graded doses of peptides ranging from 3 to 0.0001 μM. (E) MHC restriction of induced NY-ESO-1-specific CD8+ T cells was analyzed with ELISPOT assay by the addition of anti-H-2-K^d, anti-H-2-D^d or anti-H-2-L^d mAbs. These experiments were repeated two to four times with similar results. Data are mean ± SD.

the minimal epitope was identified to be NY-ESO-1$_{81-88}$ peptide (Fig. 1C).

To confirm this, graded doses of the peptides were pulsed on antigen presenting cells (APCs) and specific IFN-γ secretion was analyzed by ELISPOT assay. NY-ESO-1-specific CD8+ T cells were high-avidity, and capable to recognize as little as 30 nM of peptide (Fig. 1D), confirming that NY-ESO-1$_{81-88}$ peptide is the minimal epitope. Next, we assessed the restriction of this response using blocking antibodies. NY-ESO-1-specific CD8+ T cell responses were completely blocked by addition of anti-H-2-D^d mAb (Fig. 1E). Taken together, NY-ESO-1-specific CD8+ T cells recognize D^d-restricted NY-ESO-1$_{81-88}$ peptide.

3.2. MAGE-A4-specific CD8+ T cells recognize D^d-restricted MAGE-A4$_{265-273}$ peptide

To establish a MAGE-A4 animal model, we determined the minimal epitope of MAGE-A4-specific CD8+ T cells after immunization with MAGE-A4. Naive BALB/c mice were immunized twice at two-week intervals with plasmids encoding the entire sequence of MAGE-A4. Splenic CD8+ T cells were prepared and specific T cell responses were analyzed by ELISPOT assay using peptide pools shown in Supplementary Table 1. MAGE-A4-specific CD8+ T cells were induced in mice immunized with plasmids encoding MAGE-A4 within peptide pool #5 (Fig. 2A). To elucidate the dominant
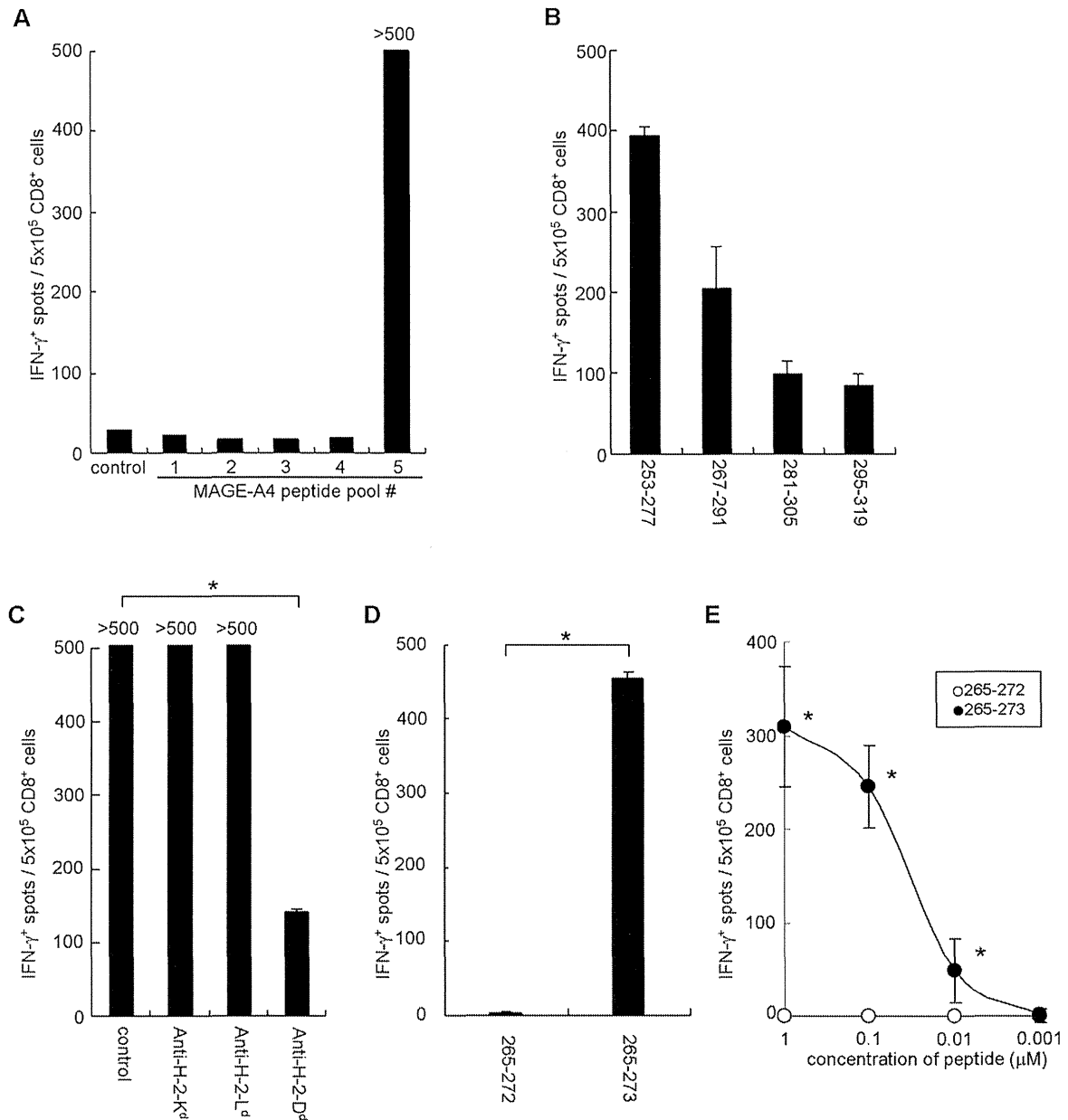
Fig. 2. MAGE-A4-specific CD8^{+} T cells recognize D^d-restricted MAGE-A4$_{265-273}$ peptide. (A, B) BALB/c mice were immunized by gene gun twice at two-week intervals with plasmids encoding the entire sequence of MAGE-A4. CD8^{+} T cells were obtained from spleens, and specific T cells were analyzed with ELISPOT assay using APCs pulsed with the indicated peptides. (C) MHC restriction of induced MAGE-A4-specific CD8^{+} T cells was analyzed with ELISPOT assay by the addition of the indicated mAb. (D) MAGE-A4$_{253-277}$ was subjected to BIMAS program and the highest score within MAGE-A4$_{253-277}$ for a D^d binding motif was predicted in 265–272 and 265–273 of MAGE-A4. These predicted peptides were analyzed with ELISPOT assay for identification of MAGE-A4 epitope peptide. (E) Avidity of MAGE-A4-specific CD8^{+} T cells was analyzed with ELISPOT assay using APCs pulsed with graded doses of peptides. These experiments were repeated two to four times with similar results. Data are mean ± SD.

MAGE-A4 epitope, MAGE-A4-specific CD8^{+} T cells were stimulated with each of the peptides from pool #5. The 253–277 peptide was most effective for stimulating MAGE-A4-specific CD8^{+} T cells (Fig. 2B). We next assessed the restriction of this response using blocking antibodies. MAGE-A4-specific CD8^{+} T cell responses were completely blocked by anti-H-2 D^d mAb (Fig. 2C). Given the H-2 D^d restriction of this CD8^{+} T cell response, we employed computer-based BIMAS program to predict optimized MHC class I epitope within the MAGE-A4$_{253-277}$ peptide. This program ranks all the possible MHC class I epitopes within a given polypeptide sequence. MAGE-A4$_{253-277}$ was subjected to this program and the highest score within MAGE-A4$_{253-277}$ for a D^d binding motif was predicted in 265–272 and 265–273 of MAGE-A4 (Supplementary Table 2). MAGE-A4-specific CD8^{+} T cells recognized the 265–273, but not

265–272 peptides, thus the minimal epitope was considered to be the MAGE-A4$_{265-273}$ peptide (Fig. 2D). To confirm this minimal epitope, graded doses of peptides were pulsed on APC and specific IFN-γ secretion was analyzed by ELISPOT assay. MAGE-A4-specific CD8^{+} T cells were high avidity, and could recognize as little as 10 nM of the peptide (Fig. 2E). We conclude that MAGE-A4-specific CD8^{+} T cells recognize D^d-restricted MAGE-A4$_{265-273}$ peptide.

3.3. Kinetics and distribution of NY-ESO-1/MAGE-A4-specific CD8^{+} T cells after gene gun immunization

Next, we generated MHC/peptide tetramers based on the data of minimal epitope and MHC restriction for NY-ESO-1/MAGE-A4-specific CD8^{+} T cells. BALB/c mice were immunized with plasmids
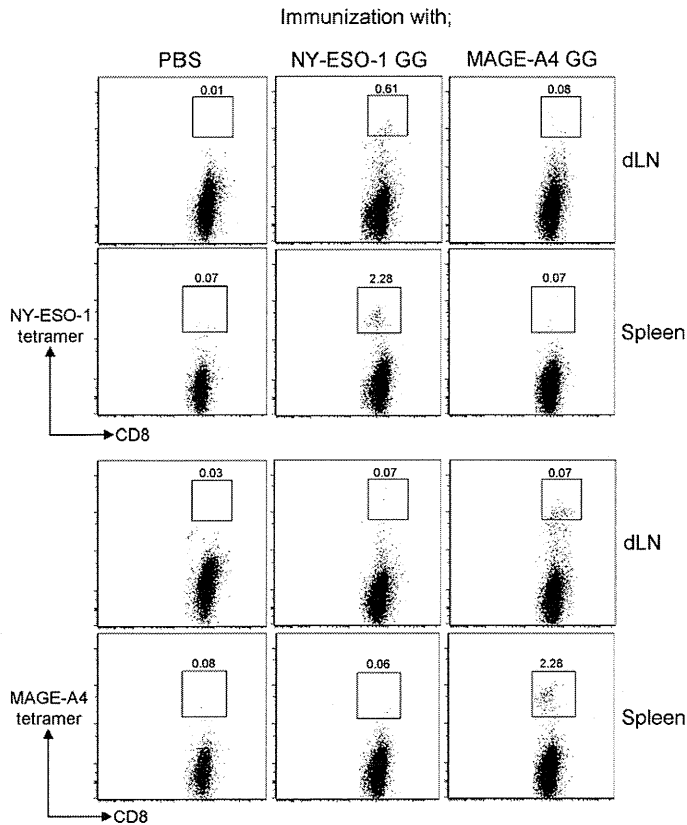
Fig. 3. NY-ESO-1/MAGE-A4-specific CD8+ T cells are detected after immunization with a gene gun. BALB/c mice were immunized twice at two-week intervals with plasmids encoding the entire sequences of NY-ESO-1 or MAGE-A4 using a gene gun. Seven days after the second vaccination, CD8+ T cells were obtained from the draining lymph nodes (dLNs) and spleens, and specific T cells were analyzed with MHC/peptide tetramer assay. These experiments were repeated two to four times with similar results. GG: gene gun.

encoding the whole sequences of NY-ESO-1 or MAGE-A4 by gene gun and the kinetics and distribution of NY-ESO-1/MAGE-A4-specific CD8+ T cells were analyzed with MHC/peptide tetramers. NY-ESO-1-specific CD8+ T cells were detected 7–10 days after the primary immunization both in draining lymph nodes and spleens in mice immunized with plasmids encoding NY-ESO-1, but not in mice immunized with MAGE-A4 or control mice (Fig. 3, 4A and 4B). NY-ESO-1-specific T cell responses were further enhanced by the secondary vaccination in both the draining lymph nodes and spleens (Fig. 4A and B). Similarly, MAGE-A4-specific CD8+ T cells were detected 7–10 days after the primary immunization by gene gun in both the draining lymph nodes and spleens and were enhanced after the booster vaccination (Figs. 3, 4C and 4D), suggesting that these assays are useful tools for analyzing the kinetics and distribution of these antigen-specific CD8+ T cells.

3.4. NY-ESO-1-specific CD8+ T cell responses are primed spontaneously after tumor inoculation and these cells partially inhibit tumor growth

It is important to establish tumor models to re-evaluate cancer immunotherapy strategies in detail. To this end, we employed CT26 (a murine colon carcinoma) tumor transplantation model with stable expression of NY-ESO-1 and examined NY-ESO-1-specific CD8+ T cell and humoral responses spontaneously primed in tumor bearing animals. BALB/c mice were inoculated with CT26-NY-ESO-1 and specific CD8+ T cell and Ab responses were analyzed with MHC/peptide tetramers and ELISA, respectively. NY-ESO-1-specific

CD8+ T cells were spontaneously primed 7 days after tumor inoculation in the draining lymph nodes, spleens and peripheral blood in mice inoculated with CT26-NY-ESO-1 and augmented thereafter (Fig. 5A). We then addressed whether these spontaneously-primed NY-ESO-1-specific CD8+ T cells were involved in tumor growth inhibition. To deplete these CD8+ T cells, tumor bearing mice were injected with anti-CD8 mAb and tumor growth was analyzed. Anti-CD8 mAb administration augmented tumor growth compared with the control group without any treatment (Fig. 5C), suggesting an anti-tumor role of spontaneously-primed NY-ESO-1-specific CD8+ T cells. On the other hand, NY-ESO-1-specific Ab responses were not observed 7 days after tumor inoculation, but detected 21 days after tumor inoculation (Fig. 5B). This is compatible with immunological monitoring in humans showing that higher stage of melanoma patients frequently develop humoral immune responses against NY-ESO-1 [3,14].

We next immunized these mice with plasmids encoding the entire sequence of NY-ESO-1 and anti-tumor activity was examined. Tumor growth was significantly reduced by immunization with NY-ESO-1 as compared to the control group without treatment (Fig. 5C). Furthermore, CD8+ T cell depletion totally abolished the anti-tumor effects induced by DNA vaccine (Fig. 5C). As CD4+ regulatory T cells (Tregs) are reportedly associated with spontaneously-primed and treatment-induced anti-tumor immune responses [15], we also investigated tumor-infiltrating Tregs. While Tregs were present in tumors, their frequency was not associated with anti-tumor activity induced by immunization with plasmids encoding NY-ESO-1 (Fig. 5D). Together, CD8+ T cell and Ab responses to NY-ESO-1 in this tumor model closely parallel NY-ESO-1 immune responses in humans. Spontaneous tumor antigen-specific immune responses restrained, albeit incomplete, tumor growth, but tumor growth were vigorous and overwhelmed the tumor growth inhibition, thus additional augmentation of these immune responses are required for effective control of tumor growth.

3.5. MAGE-A4-specific CD8+ T cell responses is primed spontaneously after tumor inoculation

We established another tumor transplantation model with stable expression of MAGE-A4 and examined MAGE-A4-specific CD8+ T cell and humoral responses spontaneously primed in tumor bearing mice. BALB/c mice were inoculated with CT26-MAGE-A4 and specific CD8+ T cell and humoral responses were analyzed with MHC/peptide tetramers and ELISA. In these mice, MAGE-A4-specific CD8+ T cells were spontaneously primed 7 days after tumor inoculation in the draining lymph nodes, spleen and PBMC, and augmented thereafter (Fig. 6A). MAGE-A4-specific Ab responses were not observed 7 days after tumor inoculation, but detected 21 days after tumor inoculation (Fig. 6B). Like as the result of NY-ESO-1 models, cellular and humoral immune responses to MAGE-A4 in this model closely parallel MAGE-A4 immune responses in humans.

4. Discussion

We have established mouse models that allowed studies on NY-ESO-1 and MAGE-A4 immunity. Using these models, we evaluated the kinetics and distribution of antigen-specific CD8+ T cells after tumor growth and immunization. While it has been recently shown that CD4+CD25+ Tregs and the ratio of CD8+ effector T cells to Tregs in tumors critically influenced the prognosis of cancer patients [16,17], limitation of samples usually makes it difficult to investigate the function of effector T cells and Tregs at tumor sites in humans. Given the importance of tumors as active sites of anti-tumor responses, it is important to examine not only the draining
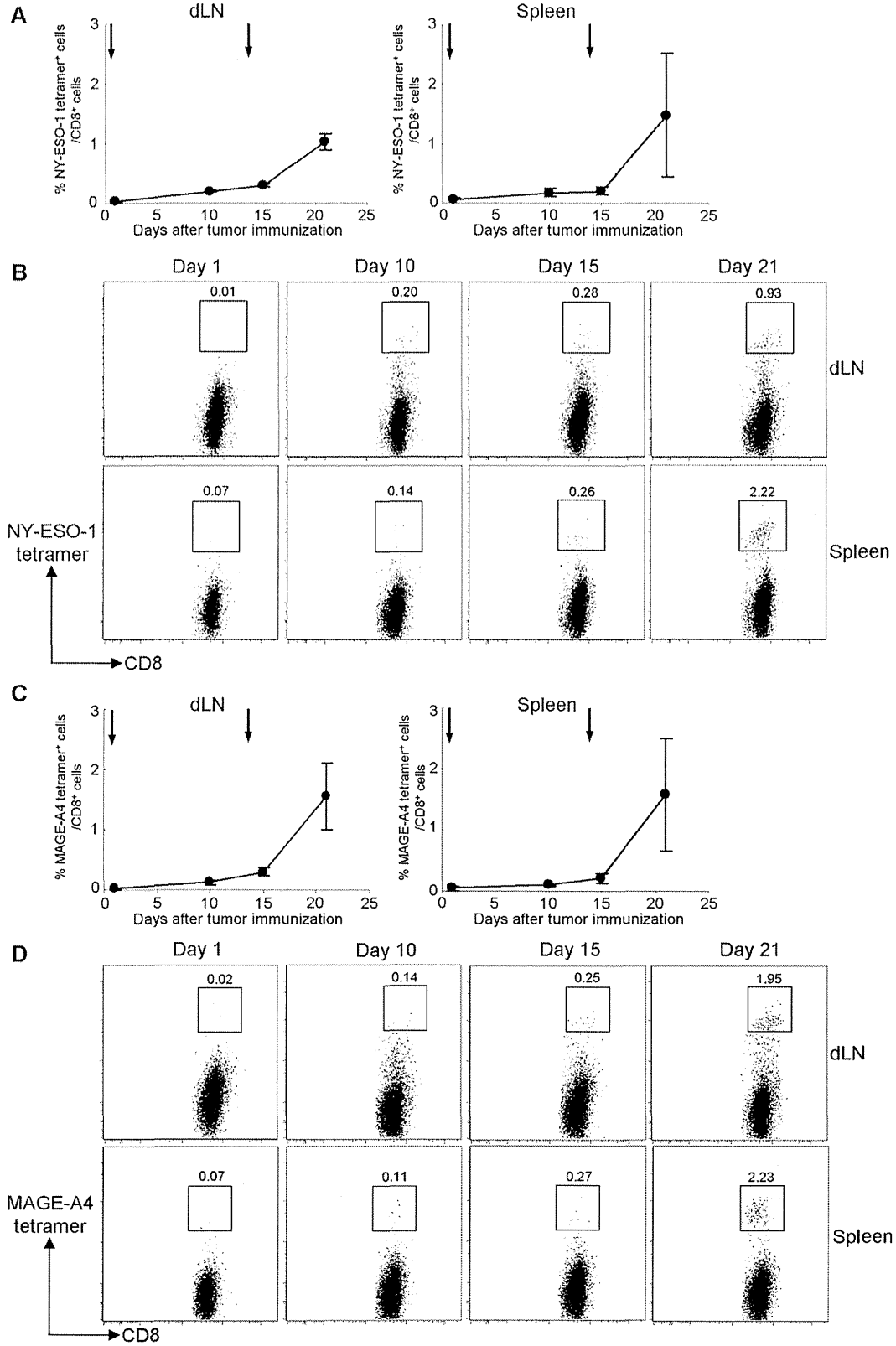
Fig. 4. Kinetics and distribution of NY-ESO-1/MAGE-A4-specific CD8⁺ T cells after immunization with a gene gun. Kinetics and distribution of NY-ESO-1 (A and B)/MAGE-A4 (C and D)-specific CD8⁺ T cells were analyzed by MHC/peptide tetramer assay. BALB/c mice were immunized twice at two-week intervals with plasmids encoding the entire sequence of either NY-ESO-1 or MAGE-A4 using a gene gun. CD8⁺ T cells were obtained from the draining lymph nodes (dLNs) and spleens on the indicated days, and specific T cells was analyzed with MHC/peptide tetramer assay. These experiments were repeated two to four times with similar results. Data in (A) and (C) are mean ± SD. Arrows in (A) and (C) represent the first and second immunization.
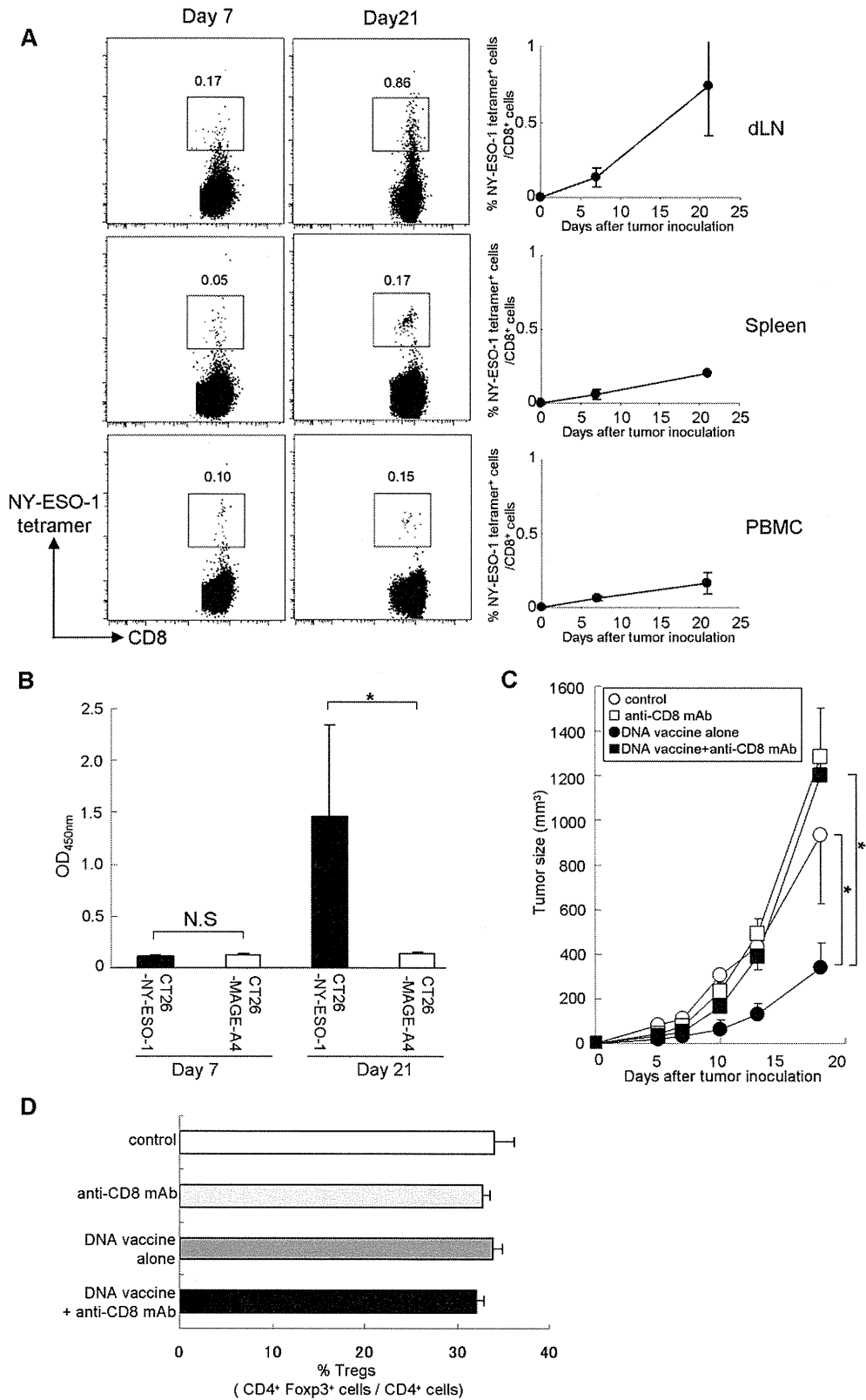
Fig. 5. NY-ESO-1-specific CD8+ T cells are primed spontaneously after tumor inoculation, and these cells partially inhibit tumor growth. BALB/c mice were inoculated with CT26-NY-ESO-1. (A) CD8+ T cells were isolated from the draining lymph nodes (dLNs), spleens and PBMCs on the indicated days, and NY-ESO-1-specific T cells were analyzed with MHC/peptide tetramer assay. (B) Sera were obtained on the indicated days and Ab responses against NY-ESO-1 were analyzed with ELISA. These experiments were repeated twice with similar results. Data are mean ± SD. *$p < 0.05$ as compared to control. (C) BALB/c mice were immunized with plasmids encoding the entire sequence of NY-ESO-1, and CT26-NYESO-1 was inoculated on day 21 (one week after final immunization). Indicated groups of mice were administered with anti-CD8 mAb (clone 19/178, 100 μg/mouse, every 12 days). More than 95% of CD8+ T cells were depleted by this method (data not shown). Each group consisted of four mice. Mice were monitored thrice a week. These experiments were repeated two times with similar results. (D) Tumor infiltrating lymphocytes were collected 21 days after tumor inoculation and the frequency of Foxp3+ cells in CD4+ T cells was analyzed.
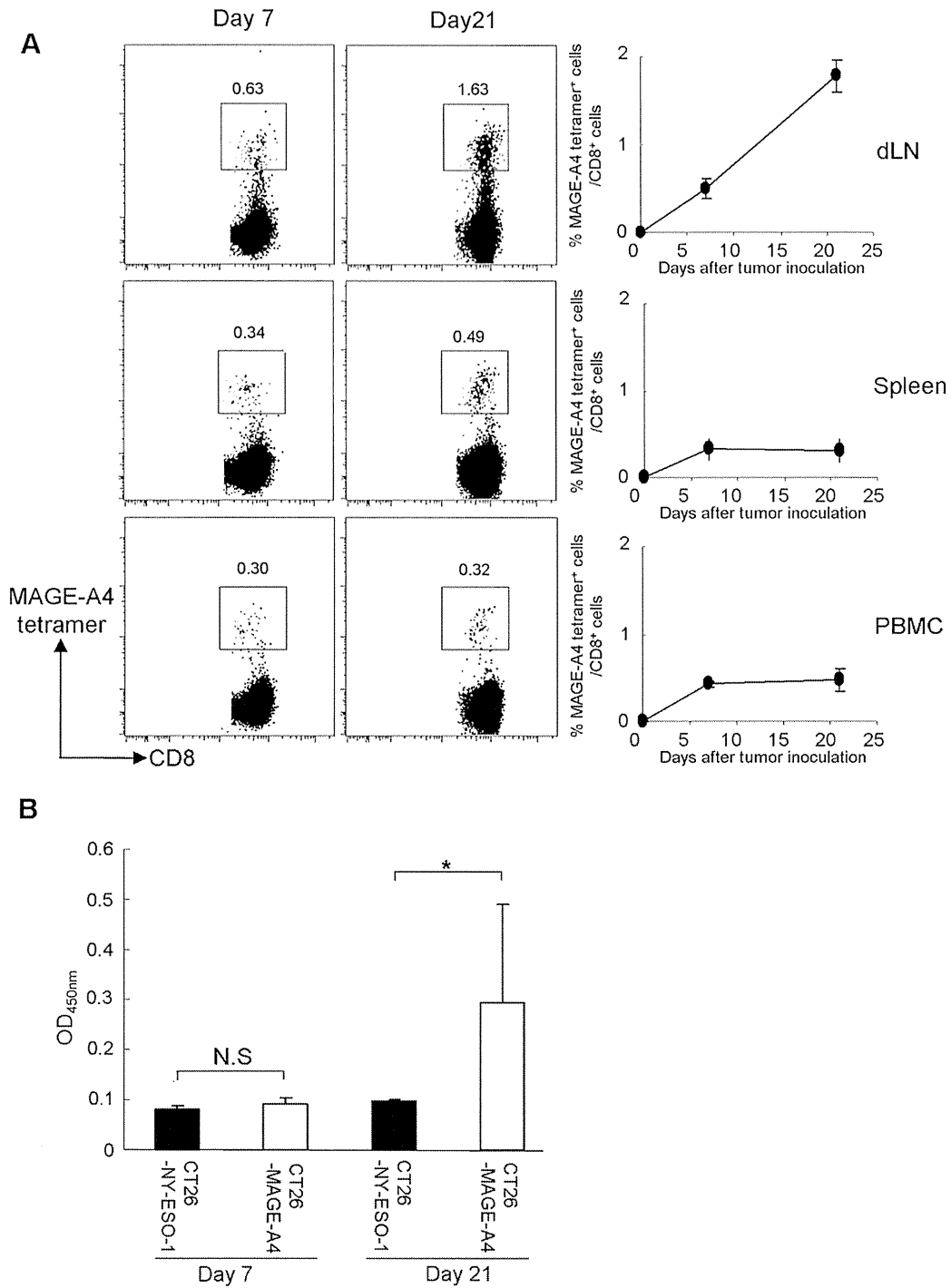
Fig. 6. Spontaneous MAGE-A4-specific CD8+ T cells are primed after tumor inoculation. BALB/c mice were inoculated with CT26-MAGE-A4. (A) CD8+ T cells were isolated from the draining lymph nodes (dLNs), spleens and PBMCs on the indicated days, and MAGE-A4-specific T cells was analyzed with MHC/peptide tetramer assay. (B) Sera were obtained on the indicated days, and Ab responses against MAGE-A4 were analyzed with ELISA. These experiments were repeated twice with similar results. Data are mean ± SD. *$p < 0.05$ as compared to control.

lymph nodes, spleens and PBMCs, but also tumor local sites. Our models could be valuable tools for analyzing antigen-specific T cells in both novel cancer immunotherapy and cancer immunotherapy that have been already tested in humans.

In our models, we found that spontaneous CD8+ T cell and Ab responses were primed and increased along with tumor progression in both NY-ESO-1 and MAGE-A4 models [3,9]. Accumulating data show that induction/augmentation of anti-tumor immune responses are often detected in patients with larger tumors [3,14],

suggesting that immune responses found in our NY-ESO-1 and MAGE-A4 tumor models closely parallel NY-ESO-1 and MAGE-A4 immune responses in humans. It has been a long debate whether spontaneous anti-tumor responses detected in cancer patients impact on tumor growth, as tumors continuously grow in patients harboring spontaneous anti-tumor immune responses. Our tumor model provides a clear answer for this conundrum. Although the immune responses spontaneously primed in tumor-bearing hosts partly inhibit a tumor growth, this immune response

is not strong enough to completely reject the tumor in the host. This means that further activation of immune responses by appropriate immunotherapy is essential for tumor rejection. Indeed, when these spontaneous immune responses were augmented by DNA vaccine, tumor growth was significantly inhibited. In contrast, we have reported that peptide vaccine using this NY-ESO-1 peptide enhanced tumor growth rather than inhibiting tumor growth unless it is vaccinated with proper adjuvants [13].

In fact, antigen-specific antibody may not play an important role for tumor rejection in our models, because 1) most tumor antigens including NY-ESO-1 and MAGE-A4 focused on this study, was exclusively expressed intracellularly by the tumor cells, thus not accessible for antibody [3] and 2) Ab responses were detected on day 21, namely later than $CD8^+$ T cell responses. Nevertheless, we have reported that injection of NY-ESO-1 mAb with chemotherapy, that can accentuate the release of intracellular tumor antigens to facilitate mAb access to intracellular target molecules, augmented anti-tumor effect in the same model system, though Ab administration alone did not inhibit tumor growth [18]. In our mouse model, spontaneously-primed anti-NY-ESO-1 Ab was detected when tumors reached a larger size. The level of spontaneously-primed antibody was, however, about 10-times lower than that achieved by mAb injection [18], suggesting that spontaneously-primed Ab responses may potentially have some anti-tumor effects, but the amount of Abs is too low to exhibit effective anti-tumor activity.

Since no NY-ESO-1 homologue is present in mice, the detected immune responses against NY-ESO-1 are considered to reflect a foreign antigen, rather than a self-antigen [3]. Whereas cancer-testis antigens like NY-ESO-1 are only expressed by cancer cells and testis, but not by normal somatic cells, mimicking foreign antigens, some cancer-testis antigens are reportedly expressed in medullary thymic epithelial cells under control of AIRE (Autoimmune regulator) [3,19]. It is plausible that cancer-testis antigens like NY-ESO-1 could be considered self-antigens during thymic selection, resulting in a repertoire of NY-ESO-1-specific T cells that are either subject to central or peripheral tolerance [3,20–22]. Thus, studies using mice in which NY-ESO-1 is a self-antigen should allow resolving this issue.

A unique finding of our study is that NY-ESO-1-specific $CD8^+$ T cell epitopes were present in an immunogenic part defined in humans [3]. This finding implies that immunogenicity may be characterized with similar components between humans and mice, further supporting the usefulness of our models. Our animal models provide important tools for the development of effective cancer vaccines.

In conclusion, we established animal models involving human tumor antigens, such as NY-ESO-1 or MAGE-A4 protein. These models allowed us to study the kinetics and distribution of antigen-specific immune responses in detail, and hence providing tools to optimize the efficacy of current cancer immunotherapy.

Acknowledgments

Appendix A. Supplementary data

Supplementary data associated with this article can be found, in the online version, at http://dx.doi.org/10.1016/j.vaccine.2013.02.056.

References

[1] Scanlan MJ, Gure AO, Jungbluth AA, Old LJ, Chen Y-T. Cancer/testis antigens: an expanding family of targets for cancer immunotherapy. Immunol Rev 2002;188:22–32.

[2] Boon T, Coulie PG, Van den Eynde BJ, Human van der Bruggen P. T cell responses against melanoma. Annu Rev Immunol 2006;24:175–208.

[3] Gnjatic S, Nishikawa H, Jungbluth AA, Gure AO, Ritter G, Jager E, et al. NY-ESO-1: review of an immunogenic tumor antigen. Adv Cancer Res 2006;95:1–30.

[4] Belardelli F, Ferrantini M, Parmiani G, Schlom J, Garaci E. International meeting on cancer vaccines: how can we enhance efficacy of therapeutic vaccines? Cancer Res 2004;64(18):6827–30.

[5] Rosenberg SA, Yang JC, Restifo NP. Cancer immunotherapy: moving beyond current vaccines. Nat Med 2004;10(9):909–15.

[6] Chen Y-T, Scanlan MJ, Sahin U, Tureci O, Gure AO, Tsang S, et al. A testicular antigen aberrantly expressed in human cancers detected by autologous antibody screening. Proc Natl Acad Sci USA 1997;94(5):1914–8.

[7] De Plaen E, De Backer O, Arnaud D, Bonjean B, Chomez P, Martelange V, et al. A new family of mouse genes homologous to the human MAGE genes. Genomics 1999;55(2):176–84.

[8] Duffour MT, Chaux P, Lurquin C, Cornelis G, Boon T, van der Bruggen P. A MAGE-A4 peptide presented by HLA-A2 is recognized by cytolytic T lymphocytes. Eur J Immunol 1999;29(10):3329–37.

[9] Miyahara Y, Naota H, Wang L, Hiasa A, Goto M, Watanabe M, et al. Determination of cellularly processed HLA-A2402-restricted novel CTL epitopes derived from two cancer germ line genes, MAGE-A4 and SAGE. Clin Cancer Res 2005;11(15):5581–9.

[10] Nishikawa H, Tanida K, Ikeda H, Sakakura M, Miyahara Y, Aota T, et al. Role of SEREX-defined immunogenic wild-type cellular molecules in the development of tumor-specific immunity. Proc Natl Acad Sci USA 2001;98(25):14571–6.

[11] Nishikawa H, Sato E, Briones G, Chen LM, Matsuo M, Nagata Y, et al. In vivo antigen delivery by a *Salmonella typhimurium* type III secretion system for therapeutic cancer vaccines. J Clin Invest 2006;116(7):1946–54.

[12] Griswold DP, Corbett TH. A colon tumor model for anticancer agent evaluation. Cancer 1975;36(6 Suppl):2441–4.

[13] Muraoka D, Kato T, Wang LA, Maeda Y, Noguchi T, Harada N, et al. Peptide vaccine induces enhanced tumor growth associated with apoptosis induction in $CD8^+$ T cells. J Immunol 2010;185(6):3768–76.

[14] Jager E, Stockert E, Zidianakis Z, Chen Y-T, Karbach J, Jager D, et al. Humoral immune responses of cancer patients against Cancer-Testis antigen NY-ESO-1: Correlation with clinical events. Int J Cancer 1999;84(5):506–10.

[15] Nishikawa H, Sakaguchi S. Regulatory T cells in tumor immunity. Int J Cancer 2010;127(4):759–67.

[16] Curiel TJ, Coukos G, Zou L, Alvarez X, Cheng P, Mottram P, et al. Specific recruitment of regulatory T cells in ovarian carcinoma fosters immune privilege and predicts reduced survival. Nat Med 2004;10(9):942–9.

[17] Sato E, Olson SH, Ahn J, Bundy B, Nishikawa H, Qian F, et al. Intraepithelial $CD8^+$ tumor-infiltrating lymphocytes and a high $CD8^+$/regulatory T cell ratio are associated with favorable prognosis in ovarian cancer. Proc Natl Acad Sci USA 2005;102(51):18538–43.

[18] Noguchi T, Kato T, Wang LN, Maeda Y, Ikeda H, Sato E, et al. Intracellular tumor-associated antigens represent effective targets for passive immunotherapy. Cancer Res 2012;72(7):1672–82.

[19] Gotter J, Brors B, Hergenhahn M, Kyewski B. Medullary epithelial cells of the human thymus express a highly diverse selection of tissue-specific genes colocalized in chromosomal clusters. J Exp Med 2004;199(2):155–66.

[20] Danke NA, Koelle DM, Yee C, Beheray S, Kwok WW. Autoreactive T cells in healthy individuals. J Immunol 2004;172(10):5967–72.

[21] Nishikawa H, Jager E, Ritter G, Old LJ, Gnjatic S. CD4+CD25+ regulatory T cells control the induction of antigen-specific CD4+ helper T cell responses in cancer patients. Blood 2005;106:1008–11.

[22] Nishikawa H, Qian F, Tsuji T, Ritter G, Old LJ, Gnjatic S, et al. Influence of CD4+CD25+ regulatory T cells on low/high-avidity CD4+ T cells following peptide vaccination. J Immunol 2006;176(10):6340–6.

Review Article

Melanoma-Targeted Chemothermotherapy and *In Situ* Peptide Immunotherapy through HSP Production by Using Melanogenesis Substrate, NPrCAP, and Magnetite Nanoparticles

Kowichi Jimbow,[1,2] Yasue Ishii-Osai,[2] Shosuke Ito,[3] Yasuaki Tamura,[4] Akira Ito,[5] Akihiro Yoneta,[2] Takafumi Kamiya,[2] Toshiharu Yamashita,[2] Hiroyuki Honda,[6] Kazumasa Wakamatsu,[3] Katsutoshi Murase,[7] Satoshi Nohara,[7] Eiichi Nakayama,[8] Takeo Hasegawa,[9] Itsuo Yamamoto,[10] and Takeshi Kobayashi[11]

[1] *Institute of Dermatology & Cutaneous Sciences, 1-27 Odori West 17, Chuo-ku, Sapporo 060-0042, Japan*
[2] *Department of Dermatology, School of Medicine, Sapporo Medical University, South 1 West 16, Chuo-ku, Sapporo 060-8556, Japan*
[3] *Department of Chemistry, School of Health Sciences, Fujita Health University, 1-98 Dengakugakubo, Kutsukake-cho, Toyoake, Aichi 470-1192, Japan*
[4] *Department of Pathology 1, School of Medicine, Sapporo Medical University, South 1 West 16, Chuo-ku, Sapporo 060-8556, Japan*
[5] *Department of Chemical Engineering, Faculty of Engineering, Kyushu University, 744 Motooka, Nishi-ku, Fukuoka 819-0395, Japan*
[6] *Department of Biotechnology, School of Engineering, Nagoya University, Furo-cho, Chikusa-ku, Nagoya 464-8603, Japan*
[7] *Meito Sangyo Co., Ltd., 25-5 Kaechi, Nishibiwajima-cho, Kiyosu, Aichi 452-0067, Japan*
[8] *Faculty of Health and Welfare, Kawasaki University of Medical Welfare, 288 Matsushimai, Kurashiki, Okayama 701-0193, Japan*
[9] *Department of Hyperthermia Medical Research Laboratory, Louis Pasteur Center for Medical Research, 103-5, Tanakamonzen-cho, Sakyo-ku, Kyoto 606-8225, Japan*
[10]*Yamamoto Vinita Co., Ltd., 3-12 ueshio 6, Tennoji-ku, Osaka 543-0002, Japan*
[11]*Department of Biological Chemistry, College of Bioscience and Biotechnology, Chubu University, 1200 Matsumoto-cho, Kasugai, Aichi 487-8501, Japan*

Correspondence should be addressed to Kowichi Jimbow; jimbow@sapmed.ac.jp

Exploitation of biological properties unique to cancer cells may provide a novel approach to overcome difficult challenges to the treatment of advanced melanoma. In order to develop melanoma-targeted chemothermoimmunotherapy, a melanogenesis substrate, N-propionyl-4-S-cysteaminylphenol (NPrCAP), sulfur-amine analogue of tyrosine, was conjugated with magnetite nanoparticles. NPrCAP was exploited from melanogenesis substrates, which are expected to be selectively incorporated into melanoma cells and produce highly reactive free radicals through reacting with tyrosinase, resulting in chemotherapeutic and immunotherapeutic effects by oxidative stress and apoptotic cell death. Magnetite nanoparticles were conjugated with NPrCAP to introduce thermotherapeutic and immunotherapeutic effects through nonapoptotic cell death and generation of heat shock protein (HSP) upon exposure to alternating magnetic field (AMF). During these therapeutic processes, NPrCAP was also expected to provide melanoma-targeted drug delivery system.

1. Introduction

The incidence of melanoma is increasing worldwide at an alarming rate [1, 2]. As yet, management of metastatic melanoma is an extremely difficult challenge. Less than 10% with metastatic melanoma patients survive currently for five years because of the lack of effective therapies [3]. There is, therefore, an emerging need to

develop innovative therapies for the control of metastatic melanoma.

The major advance of drug discovery for targeted therapy to cancer cells can be achieved by exploiting their unique biological property. The biological property unique to the melanoma cell resides in the biosynthesis of melanin pigments, that is, melanogenesis occuring within specific compartments, melanosomes. Melanogenesis begins with the conversion of amino acid, tyrosine to dopa and subsequently to dopaquinone in the presence of tyrosinase. This pathway is uniquely expressed by all melanoma cells. It is well known that the clinically "amelanotic" melanoma tissues always have tyrosinase activity to some extent, and that "in vitro amelanotic" melanoma cells become "melanotic" ones when they are regrown in the in vivo condition. Melanin precursors are inherently cytotoxic through reacting with tyrosinase to form unstable quinone derivatives [4]. Thus, tyrosine analogues that are tyrosinase substrates can be good candidates for developing drugs to melanoma-targeting therapies [5]. N-propionyl and N-acetyl derivatives (NPr- and NAcCAP) of 4-S-cysteaminylphenol, that is, sulfur-amine analogue of tyrosine, were synthesized as possible melanoma-targeted drugs (Figure 1) and found to possess selective cytotoxic effects on in vivo and in vitro melanomas through the oxidative stress that derives from production of cytotoxic free radicals by interacting with tyrosinase within melanogenesis cascade [6–10].

Intracellular hyperthermia using magnetite nanoparticles (10–100 nm-sized Fe_3O_4) may be another choice to overcome the difficult challenges for melanoma treatment. It has been shown to be effective for treating cancers in not only primary but also metastatic lesions [11, 12]. Incorporated magnetite nanoparticles generate heat (thermotherapy) within the cells after exposure to AMF due to hysteresis loss [13]. In this treatment, there is not only the heat-mediated cell death but also immune reaction due to the generation of heat shock proteins (HSPs) [14–23]. HSP expression induced by hyperthermia has been shown to be involved in tumor immunity, providing the basis for developing a cancer thermoimmunotherapy.

Based upon these rationales, we now provide evidence that melanoma-targeted chemothermotherapy can be achieved by conjugating a chemically modified melanogenesis substrate, NPrCAP with magnetite nanoparticles, which then produce apoptotic and non-apoptotic cell death through interacting with tyrosinase and heat-mediated oxidative stress; hence, immunotherapy with production of in situ peptides is being established (Figure 2).

2. Melanogenesis Substrate as a Potential Candidate for Development of Selective Drug Delivery System and Cytotoxicity to Melanoma

2.1. Synthesis of Sulfur-Amine Analogues of Tyrosine, Cysteaminylphenols, and Their Selective Incorporation into Melanogenesis Cascade. With the interaction of melanocyte-stimulating hormone (MSH)/melanocortin 1 receptor (MC1R), the melanogenesis cascade begins from activation

of microphthalmia transcription factor (MITF) for induction of either eu- or pheomelanin biosynthesis. Tyrosinase is the major player in this cascade. Tyrosinase is a glycoprotein, and its glycosylation process is regulated by a number of molecular chaperons, including calnexin in the endoplasmic reticulum [24, 25]. Vesicular transport then occurs to carry tyrosinase and its related proteins (TRPs) from trans-Golgi network to melanosomal compartments, which appear to derive from early and late endosomal compartments. In this process a number of transporters, such as small GTP-binding protein, adaptor proteins, and PI3-kinase, play important roles. Once melanin biosynthesis is completed to conduct either eu- or pheomelanogenesis within melanosomes, they then move along dendritic processes and are transferred to surrounding keratinocytes in normal skin [26–28]. In metastatic melanoma cells, however, there will be practically no melanosome transfer inasmuch as there will be no receptor cells such as keratinocytes. Thus melanosomes synthesized by melanoma cells are aggregated within autophagic vacuoles in which melanogenesis-targeted drugs will be retained. In order to utilize this unique melanogenesis pathway for developing melanoma-targeted drugs, N-acetyl and N-propionyl derivatives of cysteaminylphenols (NAc- and NPrCAPs) have been synthesized [8, 29] (Figure 1).

2.2. In Vivo and In Vitro Melanocyte Toxicity and Anti-Melanoma Effects of Cysteaminylphenols (CAPs). Both NPrCAP and NAcCAP were found to selectively disintegrate follicular melanocytes after single or multiple *ip* administration to newborn or adult C57 black mice, respectively [12, 30]. In the case of adult mice after repeated *ip* administration of NPrCAP, white follicles with 100% success rate can be seen at the site where hair follicles were plucked to stimulate new melanocyte growth and to activate new tyrosinase synthesis. A single *ip* administration of NPrCAP into a new born mouse resulted in the development of silver follicles in the entire body coat. The selective disintegration of melanocytes which is mediated by apoptotic cell death can be seen as early as in 12 hr after a single *ip* administration. None of surrounding keratinocytes or fibroblasts showed such membrane degeneration and cell death [31, 32] (Figure 3).

A high, specific uptake of NAcCAP was seen *in vitro* by melanoma cell lines compared to nonmelanoma cells [9]. A melanoma-bearing mouse showed, on the whole body autoradiogram, the selective uptake and covalent binding of NAcCAP in melanoma tissues of lung and skin [6]. The specific cytotoxicity of NPrCAP and NAcCAP was examined on various types of culture cells by MTT assay, showing that only melanocytic cells except HeLa cells possessed the low IC50 [8, 9]. The cytotoxicity on DNA synthesis inhibition was timedependent and irreversible on melanoma cells but was transient on HeLa cells [10].

The *in vitro* culture and *in vivo* lung metastasis assays showed the melanoma growth can be blocked by administration of NAcCAP combined with buthionine sulfoximide (BSO), which blocked the effect of antioxidants through reducing glutathione levels. There was a marked growth inhibition of cultured melanoma cells in the presence of BSO
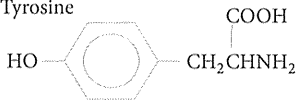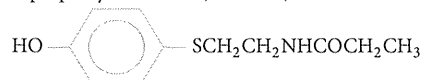
	Km (μM)	V_{max} (μmole/min/mg)
Tyrosine COOH HO—⟨⟩—CH$_2$CHNH$_2$	0.3	1.8
N-acetyl-4-S-CAP (NAcCAP) HO—⟨⟩—SCH$_2$CH$_2$NHCOCH$_3$	375	9.28
N-propionyl-4-S-CAP (NPrCAP) HO—⟨⟩—SCH$_2$CH$_2$NHCOCH$_2$CH$_3$	340.9	5.43

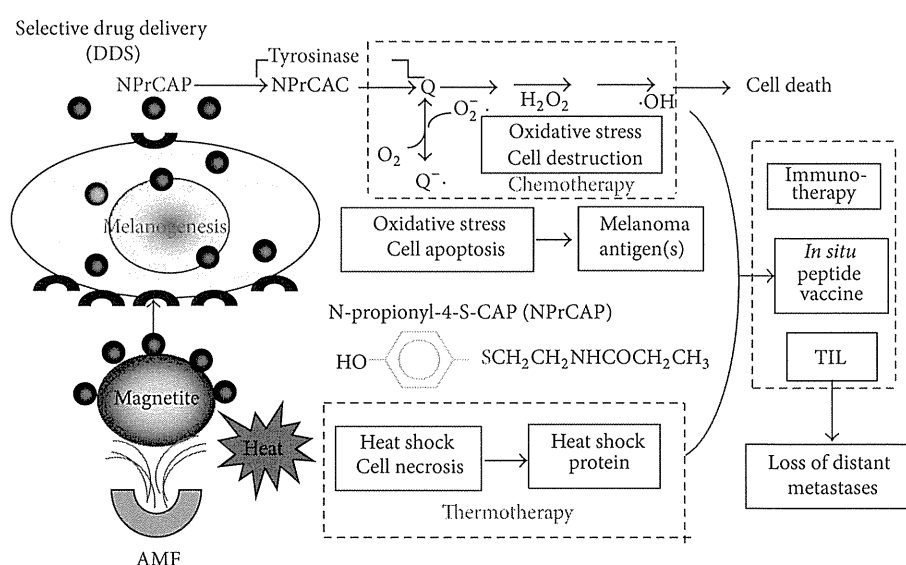FIGURE 1: Synthesis and chemical structures of NAcCAP and NPrCAP and their tyrosinase kinetics.

FIGURE 2: Strategy for melanogenesis-targeted CTI and *in situ* peptide vaccine therapy by conjugates of NPrCAP and magnetite nanoparticles with AMF exposure.

indicating that the selective cytotoxicity by CAP is mediated by the production of cytotoxic free radicals. The *in vivo* lung metastasis experiment also showed the decreased number of lung melanoma colonies [6]. The problem was, however, that a fairly large number of amelanotic melanoma lesions were seen to grow in the lung [6]. NPrCAP has been developed and conjugated with magnetite nanoparticles in the hope of increasing the cytotoxicity and overcoming the problem.

3. Conjugation of NPrCAP with Magnetite Nanoparticles and *In Vivo* Evaluation of Melanoma Growth Inhibition with/without Thermotherapy

3.1. Synthesis for Conjugates of NPrCAP with Magnetite Nanoparticles and Their Selective Aggregation in Melanoma for

Development of Chemo-Thermo-Immunotherapy. Magnetite nanoparticles have been employed for thermotherapy in a number of cancer treatments including human gliomas and prostate cancers [33–35]. They consist of 10–100 nm-sized iron oxide (Fe$_3$O$_4$) with a surrounding polymer coating and generate heat when exposed to AMF [12]. We expected the combination of NPrCAP and magnetite nanoparticles to be a potential source for developing not only antimelanoma pharmacologic but also immunogenic agent. Based upon the melanogenesis-targeted drug delivery system (DDS) of NPrCAP, NPrCAP/magnetite nanoparticles complex was expected to be selectively incorporated into melanoma cells. It was also hypothesized that the degradation of melanoma tissues may occur from oxidative and heat stresses by exposure of NPrCAP to tyrosinase and by exposure of magnetite nanoparticles to AMF. These two stress processes may then produce the synergistic or additive effect for generating

tumor-infiltrating lymphocytes (TIL) by *in situ* formation of peptides that will kill melanoma cells in distant metastases (Figure 2).

In order to develop effective melanoma-targeted chemotherapy (by NPrCAP) and thermo-immunotherapy (by magnetite nanoparticles with HSP), hence providing a basis for chemo-thermo-immunotherapy (CTI therapy), we synthesized conjugates of NPrCAP and magnetite nanoparticles, on which NPrCAP is bound directly or indirectly on the surface of magnetite nanoparticles or magnetite-containing liposomes (Figure 4). Among these NPrCAP and magnetite complexes listed in Figure 4, NPrCAP/M and NPrCAP/PEG/M were chemically stable, did not lose biological property, and could be filtered as well as easily produced in large quantities. Most of the experiments described below were carried out by employing the direct conjugate of NPrCAP and magnetite nanoparticles, NPrCAP/M. A preliminary clinical trial, however, used NPrCAP/PEG/M to which polyethylene glycol (PEG) was employed to conjugate NPrCAP and magnetite nanoparticles.

In our studies, we found that NPrCAP/M nanoparticle conjugates were selectively aggregated in melanoma cells compared to non-melanoma cells [36]. The conjugates of NPrCAP and magnetite nanoparticles would be selectively aggregated on the cell surface of melanoma cells through still unknown surface receptor and then incorporated into melanoma cells by early and late endosomes. The conjugates were then incorporated into melanosomal compartment as the stage I melanosomes derive from late endosome-related organelles, to which tyrosinase was transported from the trans-Golgi network by vesicular transport [26].

3.2. In Vivo Growth Inhibition of Mouse Melanoma by Conjugates of NPrCAP and Magnetite Nanoparticles with/without Thermotherapy. The intracellular hyperthermia using magnetic nanoparticles is effective for treating certain types of primary and metastatic cancers [11, 12, 35–39]. Incorporated magnetic nanoparticles generate heat within the cells after exposure to the AMF due to hysteresis loss or relaxational loss [13, 40]. In our study of B16 melanoma cells using B16F1, B16F10, and B16OVA cells, we compared the thermo-therapeutic protocols in detail by evaluating the growth of the rechallenge melanoma transplants as well as the duration and rates of survival of melanoma-bearing mice.

By employing B16F1 and F10 cells, we first evaluated the chemotherapeutic effect of NPrCAP/M with or without AMF exposure which generates heat. NPrCAP/M without heat inhibited growth of primary transplants to the same degree as did NPrCAP/M with heat, indicating that NPrCAP/M alone has a chemotherapeutic effect. However, there was a significant difference in the melanoma growth inhibition of re-challenge transplants between the groups of NPrCAP/M with and without heat. NPrCAP/M with AMF exposure showed the most significant growth inhibition in re-challenge melanoma transplants and increased life span of the host animals, that is, almost complete rejection of re-challenge melanoma growth, whereas NPrCAP/M without heat was

much less, indicating that NPrCAP/M with heat possesses a thermo-immunotherapeutic effect (Figures 5(a), 5(b), and 5(c)).

Specifically our study indicated that the most effective thermoimmunotherapy for re-challenge B16F1 and F10 melanoma cells can be obtained at a temperature of 43°C for 30 min with the treatment repeated three times on every other day intervals without complete degradation of the primary melanoma [37]. This therapeutic approach and its biologic effects differ from those of magnetically mediated hyperthermia on the transplanted melanomas reported previously. In previous studies by Suzuki et al. [38] and Yanase et al. [39], cationic magnetoliposomes were used for B16 melanoma. They showed that hyperthermia at 46°C once or twice led to regression of 40–90% of primary tumors and to 30–60% survival of mice, whereas their hyperthermia at 43°C failed to induce regression of the secondary tumors and any increase of survival in mice [38, 39].

4. Production of Heat Shock Protein, Nonapoptotic Cell Death, and Tumor-Infiltrating Lymphocytes by Conjugates of NPrCAP and Magnetite Nanoparticles with Thermotherapy

4.1. Production of Heat Shock Protein and Non-Apoptotic Melanoma Cell Death by NPrCAP/Magnetite Nanoparticle Conjugates with Thermotherapy. It has been shown that hyperthermia treatment using magnetite cationic liposomes (MCLs), which are cationic liposomes containing 10-nm magnetite nanoparticles, induced antitumor immunity through HSP expression [12, 22, 41, 42]. In our studies using B16F1, F10, and OVA melanoma cells [43], the hyperthermia using NPrCAP/M with AMF exposure also showed antitumor immune responses via HSP-chaperoned antigen (Figure 6) [43]. It may be speculated that the HSPs-antigen peptide complex released from melanoma cells treated with this intracellular hyperthermia is taken up by dendritic cells (DCs) and cross-presented HSP-chaperoned peptide in the context of MHC class I molecules [44]. In our CTI therapy with AMF exposure, the heat-mediated melanoma cell necrosis was induced to NPrCAP/M-incorporated cells. In this group, we also found that repeated hyperthermia (3 cycles of NPrCAP/M administration and AMF irradiation) was required to induce the maximal antitumor immune response [37].

If melanoma cells escaped from this necrotic cell death, repeated hyperthermia should produce further necrotic cell death to the previously heat-shocked melanoma cells in which HSPs were induced. Our CTI therapy with AMF exposure using B16OVA cells showed that Hsp72/Hsc73, Hsp90, and ER-resident HSPs participated in the induction of CD8$^+$ T-cell response [43]. Different from the results of B16F1 and F10 cells, Hsp72 was largely responsible for the augmented antigen presentation to CD8$^+$ T cells. As Hsp72 is known to upregulate in response to hyperthermia or heat shock treatment [41], newly synthesized Hsp72 has a chance to bind to the heat-denatured melanoma-associated antigen.